Spatial propagation of temperate phages within and among biofilms

James B. Winans[1], Sofia L. Garcia[1], Lanying Zeng[2], Carey D. Nadell[1*]

1. Department of Biological Sciences, Dartmouth, Hanover, NH

2. Department of Biochemistry and Biophysics, Center for Phage Technology, Texas A&M University, College Station, TX

* Author for correspondence:

Carey Nadell (ORCID 0000-0003-1751-4895)

carey.d.nadell@dartmouth.edu

78 College St., Rm. 326

Dartmouth, Dept. of Biological Sciences

Hanover, NH 03755

Author contributions

JBW and CDN conceptualized the study. CDN supervised the study. JBW led protocol design and experimental development. LZ contributed key reagents. JBW and SLG performed the experiments. JBW conducted data analyses and made the figures. JBW and CDN wrote the manuscript. JBW, SLG, LZ, and CDN edited the manuscript.

Abstract

Bacteria form groups comprised of cells and secreted adhesive matrix that controls their spatial organization. These groups – termed biofilms – can act as refuges from environmental disturbance and from biotic threats, including phages. Despite the ubiquity of temperate phages and bacterial biofilms, temperate phage propagation within biofilms has never been characterized on multicellular spatial scales. Here, we leverage several approaches to track temperate phages and distinguish between lytic and lysogenic infections. We determine that lysogeny within *E. coli* biofilms most often occurs within a predictable region of cell group architecture. Because lysogens are generally found on the periphery of large groups, where lytic viral activity also reduces local structural integrity, lysogens are predisposed to disperse and are over-represented in biofilms formed downstream of the original biofilm-phage system. Comparing our results with those for virulent phages reveals that the temperate phages possess previously unknown advantages for propagation in architecturally heterogeneous biofilm communities.

Introduction

Across large ranges in spatial scale and phylogenetic distance, many species - from microbes to the largest metazoans - form groups as an adaptive strategy to navigate environmental challenges (*1–5*). Microbial collectives, often termed biofilms, are produced either in a free-floating state or attached to surfaces. Biofilms are primarily composed of cells and a suite of secreted adhesive polymers, called the extracellular matrix(*6–8*). This mode of group formation among bacteria is ubiquitous in both natural and human-made environments, and a primary function of collective growth is protection against invading competitors, diffusible antimicrobial compounds, predatory bacteria, and phages(*9–11*). The cellular scale dynamics of group protection against these threats are not well known, particularly for phages and predatory bacteria(*12–15*). Complementing prior work with cellular scale observation of phage-biofilm interactions can provide crucial insight into the driving mechanisms of these interactions at the scale on which microbial phenotypes directly manifest.

Different microbial predators have a diversity of life history patterns. Obligate lytic phages, also called virulent phages, inject their genome into host cells, where the cellular machinery is coopted for phage replication preceding host cell lysis(*16*). Temperate phages, by contrast, have two different modes of propagation: 1) they may proceed with a lytic infection similar to that of virulent phages, killing the host cell and producing a new burst of phage virions, or 2) they may integrate into the bacterial genome or persist as an episome to generate a host lysogen that carries the phage's genome along with it as it undergoes normal growth and division(*17*). Once integrated into a host's genome, prophages can introduce new genes that substantially alter cell physiology, including antibiotic resistance, metabolic capacity, and virulence(*18–21*). Additionally, the movement of temperate phages into and out of host genomes often mediates horizontal gene transfer(*22*); has powerful, ancient, and widespread effects on microbial evolution (*23*, *24*); and can drive lysogenic conversion of pathogens that present major challenges to human health(*25*). An enormous wealth of knowledge of phage ecology, evolution, and molecular genetics has been gathered over a century of research(*16*, *26–30*). However, despite the ubiquity of biofilms and phages in microbial ecology, we are still learning the fundamentals of how phages interact with biofilm-dwelling hosts. Temperate phage propagation, in particular, remains uncharacterized at cellular and multicellular spatial scales among host bacteria in biofilms.

Recent work has begun to clarify the fundamentals of lytic phage propagation at high spatial and temporal resolution in the biofilm context. This research has shown that, for several species, bacteria within biofilms are often protected from lytic phage exposure(*31–35*), and that this protection is dependent on biofilm growth and architectural maturity at the time of phage introduction. When *E. coli* is growing in a biofilm context, for example, the hosts' interactions with lytic phages are profoundly different relative to shaken liquid culture conditions(*12*, *31*, *36*). Mature *E. coli* biofilms can maintain net-positive growth in the presence of T7 phages by blocking phage diffusion in a manner dependent on the secretion of curli amyloid fibers(*31*), a core proteinaceous component of the *E. coli* biofilm matrix. Phages can be trapped within the networks of highly packed cells and curli fiber protein on the periphery of the biofilm, but the phages remain viable and can infect susceptible bacteria attempting to colonize the biofilm exterior from the planktonic phase(*36*). The spatial constraint of biofilms inherently tends to create negative frequency-dependent selection for conventional genetic phage resistance, as resistant cells, once they are common, further reduce phage mobility in the system and can prevent susceptible cells from being exposed and infected(*37*, *38*).

The existing work summarized above has established an early picture of how obligate lytic phages interact with biofilm-dwelling hosts at the cellular scale on which bacterial and phage phenotypes directly manifest. In contrast, there is very little analogous work on how temperate phages propagate through biofilm populations and communities, and how the patterns of activity at microbial community scale are driven by cellular scale interaction dynamics. Some prior work has used traditional macroscopic measurements to explore how temperate phage exposure influences biofilms (*39*). A recent study showed that non-specific genome insertion by prophages can accelerate bacterial evolution by increasing host mutation rate in biofilms of *P. aeruginosa* (*40*). Other work with lambdoid phage H-19B and *E. coli* MG1655 indicated that almost all host cells are quickly lysogenized in biofilm populations (*41*). These works set a precedent that temperate phage exposure in biofilms can be important; but efforts thus far have used techniques that disrupt the physical architecture of the biofilms and average over the entire host and phage populations. Crucial questions therefore remain: how do temperate

phages propagate through biofilms at the cellular scale; how do these fine-scale patterns influence population and community structure and composition, and how are the answers to these questions distinct for temperate phages relative to obligate lytic phages(*42*)? Additionally, why do different temperate phages have varying strategies for the lytic/lysogenic switch, or how might this affect their biofilm-scale propagation in relation to spatial variation in cell physiological state and biofilm architecture (*22*, *43*, *44*)?

To begin answering these questions, we developed a model system in which host bacteria can be visualized at single cell resolution, naïve — that is, uninfected — cells can be distinguished from lysogenized hosts, and phage virions can also be visualized. The model comprises monoculture biofilms of *E. coli* AR3110 cultivated in microfluidic devices under constant media flow, to which either temperate phage λ (or, in selected control experiments, obligate lytic phage T7 or λΔ*cI*) can be added at any time during or after host cell surface colonization, cell growth, and biofilm matrix secretion. *E. coli* is among the most extensively studied organisms in microbiology, and its mechanisms of biofilm formation have likewise been dissected thoroughly (*45*–*52*). Similarly, temperate phage λ has been studied in detail over many decades of work (*53*–*63*). Here, we assess how this phage and its host interact within biofilms at the resolution of individual cells and phage virions. Our study yields new insight into the fundamental principles of temperate phage propagation at cellular scales, the impact of the temperate phage life history strategy on host biofilm architecture, and the nature of local versus distal dispersal-based spread of temperate versus virulent phages within and among biofilms.

Results

E. coli AR3110 was engineered to constitutively produce the fluorescent protein mKate2. We note that this strain, AR3110, is a K-12 derivative with biofilm matrix production restored relative to the parental W3110 K-12 lineage(*45*). The resulting strain was used to inoculate microfluidic devices composed of glass coverslips bonded to polydimethylsiloxane molds **(S1 Fig)**. After a 45-min period of stationary conditions to allow cells to attach to the glass substratum, M9 minimal media with 0.5% maltose as the sole carbon source was introduced at 0.1 μL min^{-1} (average flow velocity = 45 μm/s) for 48 h. The media influent was then switched to a new syringe with the same growth media plus λ phages at a concentration of 10^4 PFU μL^{-1} for 24 h. This strain of λ, λLZ1367, has a copy of mTurquoise2 translationally fused to λD, which encodes the capsid decorative protein gpD that assembles more than 400 copies per virion head and is required for λ stabilization(*64*, *65*). λLZ1367 also contains a downstream transcriptional fusion of mKO2 to the *cI* locus encoding Repressor, which causes lysogenized hosts to produce the fluorescent protein mKO2(*65*–*67*). Overall, this arrangement of constitutive and regulated fluorescent protein constructs on the bacterial and phage genomes allows for cellular resolution spatial tracking of non-lysogenized hosts (mKate2), lysogenized hosts (mKO2), as well as λ phages (mTurquoise2). We confirmed that phage fluorescence scales linearly with phage count in our image data, and that production of mKO2 provides highly accurate measurement of lysogenization frequency for all experiments below (**S2 Fig).**

Early phage propagation and host lysogenization occur along the biofilm periphery

As biofilms increase in size under flow, cells may detach actively or passively from existing groups, re-attach elsewhere in the chamber, and begin producing new cell groups. As a result, after 48 h of incubation prior to adding phages, our biofilm chambers contained a variety of *E. coli* host cell groups of different size and packing architecture (**S3 Fig)**. In this culture condition, the largest and longest-established clusters of *E. coli* are each composed of a densely packed center, surrounded by cells with lower packing density (**S3 Fig**). Spatial heterogeneity in cell state (unexposed, lysed, lysogenized) arose quickly after phages were added to biofilms. On short time scales, per expectation, the predominant mode of phage propagation was through lytic events in which phages produced a new burst of phage virions. We found that small groups of up to ~100 cells were mostly lysed and removed from the surface. Larger clusters of *E. coli* were commonly found to have a peripheral region containing many λ phages, newly formed lysogens, and naïve host cells, as well as a protected, highly packed central core of cells with minimal detectable presence of phages and no lysogenized hosts (**Figure 1A-B**). Direct quantification demonstrates that phages are indeed restricted to the outer layers of cell groups (**S4 Fig).**

To determine whether the naïve *E. coli* cells that survived and remained uninfected did so due to *de novo* evolution of resistance to phage λ, we repeated the experiment above, but after introducing λ for 24 h, all of the cells within the microfluidic device were flushed out and plated for resistance to λ infection (See Methods). The frequency of λ resistance in this surviving *E. coli* population was approximately 10^{-5}, which is not significantly different from the background frequency of resistant mutants in our overnight cultures prior to any phage exposure (**S5 Fig)**. This result indicates that *de novo* genetic λ resistance did not contribute to the population dynamics in our experiments, and it is consistent with the fact that our biofilm cultures contain bacterial and phage population sizes and contact rates that, due to spatial constraint, are orders of magnitude lower than those found in shaken liquid batch culture(*12*, *31*, *36*). The results above instead suggest – consistent with our prior work exploring T7 phage propagation – that *E. coli* biofilm architecture can limit the diffusion of phages to a region along the periphery of cell groups and effectively create a refuge against phage exposure in its core region that is stable through time(*12*, *31*). Again, consistent with prior work, the biofilm architecture that leads to overall phage protection only occurs if *E. coli* has sufficient time to grow prior to the introduction of phages; if phages are introduced from the beginning of biofilm growth, the spatial pattern of naïve cell distribution, cell packing, phage diffusion, and lysogen localization shown in Figure 1 does not occur (**S6 Fig**).

Our observations above suggested that for *E. coli* biofilms of sufficient size and architectural maturity, temperate phage propagation can occur along the peripheral regions of cell clusters, where cell packing is lowest. In general, cell packing increases with distance from the biofilms' outer surface (**S4 Fig**); we will use cell packing as the key index for this study, as cell packing, rather than distance from biofilm exterior, is more directly mechanistically linked to phage localization (see below). The lytic activity of the phages tends to reduce local cell packing even further, and it is within this region of reduced cell density that lysogenization is observed. To assess this visual intuition quantitively, we used the BiofilmQ analysis framework to calculate the distribution of lysogenized cells with respect to local packing density and to compare their distribution with that of the total *E. coli* population (See Methods, **S7 Fig**). We find that lysogens are in fact over-represented in biofilm regions with lower packing density and are heavily skewed in this respect compared to the background total distribution of cell packing within large *E. coli* biofilm colonies (**Fig 1E**)**.** This pattern was consistent across repeated runs of the experiment: the cell packing of areas occupied by lysogens was consistently lower than that of the entire *E. coli* population on average (**Fig 1F**). We also found that the variance in local cell packing in regions occupied by lysogens was consistently lower than the cell packing distribution of the total host cell population, emphasizing our observation that the spatial constraints with which phages encounter host biofilm structures intrinsically cause lysogens to be produced in peripheral, low-density regions of *E. coli* cell groups **(Fig 1G)**.

These results suggested to us that the consistent spatial patterning of lysogenization was due to the ability of *E. coli* to create biofilms with high cell packing architecture, which ultimately blocks phage diffusion into the highly packed core regions of larger host biofilm colonies. Previous research documenting halted diffusion of T7 phages into *E. coli* biofilms showed that this protective phage blocking was a function of the packing structure generated by the secretion of curli matrix proteins(*31*). A difference we observe here is that *E. coli* biofilm cell groups become larger with rougher surface topography in our media conditions (M9 minimal with 0.5% maltose), as opposed to the flat mat architecture seen in the prior study of T7 diffusion in *E. coli* biofilms (which was done in 1% tryptone broth). To further clarify this point, we used a previously engineered strain of *E. coli* which has a fluorescent transcriptional reporter inserted into the *csgBAC* operon that encodes the proteins for curli assembly(*31*). We observe a non-monotonic relationship between cell density and curli transcription (**S8 Fig)**. We repeated these experiments with an *E. coli* strain that has a 6xHIS tag fused to the csgA monomer, which allows for immunostaining of the curli biofilm matrix. This tag has been shown to not interfere with the formation or functionality of the curli matrix(*31*). We observe a similar relationship between cell density and curli immunostaining as we did with the transcription reporter (**S8 Fig**). We reasoned that if curli matrix production is necessary for creating biofilm regions that are inaccessible to phages, a mutant strain of *E. coli* lacking the ability to produce curli should produce biofilms in which all cells are phage-accessible and lysogens should arise relatively homogeneously throughout the system. We tested this possibility by repeating the experiments above using a strain of *E. coli* (denoted Δ*csgBA*) harboring deletions of *csgB* (encoding the curli baseplate) and *csgA* (encoding the curli amyloid monomer). We grew biofilms of the Δ*csgBA* for 48 h prior to adding phages; after a further 24 h, we observed that phages and lysogens could be found throughout the host biofilm, as anticipated (**Fig 1C-D**). The inability to produce curli leads to biofilm structure with systematically lower cell packing than WT

E. coli biofilms, and the spatial distribution of lysogens relative to local cell packing exactly mirrors the distribution for the entire host cell population (**Fig 1H, S7 Fig).** Averaged over replicates of this experiment, there was no significant difference in the mean packing architecture or in the variance in packing architecture of locations occupied by lysogens compared to the total population (**Fig 1I-J**).

Lysogens saturate at low frequency in structured biofilms on multi-day time scales

Our experiments suggest that by virtue of matrix and cellular architecture in established *E. coli* biofilms, the introduction of temperate phage λ results in lytic proliferation within a finite peripheral region of sufficiently large, architecturally packed biofilm cell groups. An inevitable byproduct of this pattern is that lysogenized hosts tend to occur in the peripheral regions of large biofilm clusters (**S4 Fig**), where cell-cell packing is lower by default and is decreased further by lytic-cycle phage activity. We were next curious about the stability of these patterns through time, and how the longer-term distributions of phage lytic propagation, lysogen growth, and naïve cell growth might depend on the native biofilm matrix composition.

To explore the questions above, we grew WT *E. coli* biofilms for 48 h prior to introducing λ phages continuously for an additional 120 h, acquiring images of replicate biofilm chambers daily. The frequency of lysogens within naïve WT biofilms increased gradually before reaching a steady state at ~10% of the population after 96 h (**Fig 2A**). Given the constant influx of phages into the system, and the fact that lysogens themselves grow and divide in the peripheral regions of biofilm with highest nutrient availability, it was not immediately clear why lysogenized cells would tend to equilibrate at 10% of the population rather than continuing to increase in relative abundance. The first and obvious factor limiting lysogenization – explored in Figure 1 – is that lysogen frequency can reach an upper limit within structurally mature biofilms due to phage diffusion constraints that limit what fraction of the original naïve cell population is phage-exposed. As a result, uninfected cells residing within a highly packed cell group core can continue to replicate and keep pace with the growth of newly replicating λ lysogens found around the cell group periphery. A second explanation, not mutually exclusive from the first, is that newly formed lysogens surrounding uninfected cells could create localized secondary barriers against further phage propagation, as lysogenized cells can adsorb λ virions but are immune to superinfection(*68*, *69*). An additional explanatory factor, again not mutually exclusive from the previous two, is that newly formed lysogens might be disproportionately pre-disposed to disperse from biofilms due to their spatial arrangement on the biofilm periphery. Our next experiments indicated that all three of these factors are pertinent, with differential dispersal having further-reaching impacts that we explore in the next section.

To first assess the role of *E. coli* biofilm structure on lysogen proliferation over time, we performed the same experiment described in Figure 2A-B but used the curli-deficient Δ*csgBA* strain as the basis for the host biofilm population. Biofilms of Δ*csgBA E. coli* were again grown for 48 h without phages, and then monitored for an additional 120 h under continuous λ exposure. As observed for the WT biofilms above, lysogens initially arise slowly and after 24 h comprise only a small fraction of the total population. After 48 h, however, the relative abundance of lysogens within Δ*csgBA* host biofilms continues to increase sharply, departing more and more dramatically from the pattern seen for WT host biofilm structure. By 96 h after introduction of phages, lysogens constitute the majority of Δ*csgBA* biofilms at 80% of the total population (**Fig 2A)**. In some replicates, we observed almost 100% lysogenized cells after 96 h; more commonly, we found that lysogenized cells would constitute the majority, but with small pockets of uninfected naïve Δ*csgBA* cells remaining stable through time (**Fig 2C)**. This result suggested to us that while cell-packing architecture of WT biofilms is an essential feature explaining the trajectory of lysogen frequency, it was not the only factor leading to lysogens equilibrating below 100% of the population. We found it notable that stable patches of non-lysogenized naïve cells within otherwise fully lysogenized Δ*csgBA* host biofilms did not have phages present within them, suggesting that free λ virions might be sequestered by the lysogens around them.

To assess the adsorption of free λ phages to different host *E. coli*, we turned to well-mixed batch culture experiments in which λ phages were incubated with λ-susceptible naïve *E. coli*, λ-lysogenized *E. coli* (which can adsorb phages but do not support lytic propagation), and Δ*lamB E. coli* (which lack the LamB maltose importer to which phage λ binds, and therefore do not adsorb phage λ), or a blank media control. We began these

experiments at an initial MOI = 0.1 and tracked phage adsorption and amplification by quantifying free λ phage titer from the liquid media in each culture condition every 25 min for 5 h (see Methods). As expected, incubating phage λ in sterile media or with the Δ*lamB E. coli* deletion mutant produced no change in phage titer throughout the experiment. When we incubated λ with a previously lysogenized *E. coli* population, we observed a rapid decline in liquid phage titer that fell below the limit of detection by 200 min; this result follows expectation and recapitulates the classic superinfection immunity result that λ lysogens can rapidly sequester phages by adsorption without subsequent phage amplification(*69–71*). When we repeated this experiment with initially non-lysogenized and λ-susceptible *E. coli*, we observed an initial drop in phage titer as phages were adsorbed to host cells. However, in this condition, the initial drop in phage titer is followed by a >100-fold increase corresponding to a burst of new phages from a round of lytic infection. As explored below, a rapid increase in new *E. coli* lysogens also occurs at this time **(Fig 2D)**. From this time point forward the phage-host population dynamics are more complex, as the host *E. coli* population comprises naïve host cells and newly lysogenized hosts (both of which are actively growing), in addition to free λ phages. To better understand these dynamics, we repeated this experiment and quantified the changing abundances of lysogenized hosts and non-lysogenized naïve hosts by CFU count, in addition to monitoring free λ phage titer (see Methods). The population dynamics of the free λ phages replicated our observations from earlier trials of the experiment (Figure 2D, E). The abundance of lysogens increases sharply straight from the start of the experiment, saturating until the release of new phages from the first round of lytic infection bursts from the initially naïve *E. coli* host cell population. With the release of this new λ phage burst, lysogen abundance again increases, due to growth of existing lysogens and new lysogenization of naïve cell hosts. Surprisingly, the non-lysogenized, uninfected naïve *E. coli* cells showed variance of less than 1 order of magnitude from their inoculated population size. Our interpretation of this result is that because the naïve cells are actively replicating and partially being converted to lysogens, which adsorb free phages, their populations remain relative stable despite successive rounds of phage release, adsorption, and lysogenization or lytic amplification.

We found that by the end of this experiment at 5 h, the population frequency of lysogens was ~80%, which was similar to our experiments with the curli-deficient Δ*csgBA* background that does not impose any diffusional constraint on phage movement (**S9 Fig)**. Taken together, these results suggested to us that the steady state frequency of lysogens within naïve biofilms exposed to phages can be appropriately explained by a diffusion limitation conferred by sufficient matrix secretion and phage adsorption onto resistant lysogens once they begin to dominate the culture. This interpretation predicts that in biofilms in which cell packing architecture and the ability of lysogens to adsorb phages have been removed, phages should be able to access all infectible cells by diffusion. We tested this idea by repeating the biofilm experiment from this section with a slightly modified protocol. We cocultured Δ*csgBA* cells and a Δ*csgBA* Δ*lamB* mutant to mimic the condition in which pockets of Δ*csgBA* naïve cells grow within a majority phage-immune strain, but in this case the phage-immune strain cannot impede phage movement by adsorption. We found that after 24 h of phage inoculation, the Δ*csgBA* cells had significantly higher overlap with phage compared to the Δ*csgBA* Δ*lamB* cells (**S10 Fig)**. When we performed this same experiment with Δ*csgBA* and a Δ*csgBA* lysogenized with λ, we found no difference in phage overlap between the two strains. (**S10 Fig)** This indicates to us that phage adsorption by phage-immune cells is an important factor in maintaining a residual uninfected population in biofilm culture.

Lysogenized cells are more likely to disperse due to their characteristic spatial arrangement

So far, we have explored the process of phage propagation within individual biofilm patches as a function of the local cell packing architecture and the adsorption of phages by either naïve or lysogenized host cells as the population structure grows toward steady state. We were also curious as to the flux of dispersed cells from biofilms' exterior, particularly in light of the finding that lysogens tend to be created along the biofilm periphery. Given that lysogens are skewed in their spatial distribution toward peripheral regions of lower cell packing, and that ongoing lytic cycle activity by phage λ likely reduces local architectural packing further in the regions where lysogens are located, we speculated that lysogens are disproportionately more likely to disperse from cell groups and re-colonize elsewhere relative to their total frequency in biofilms.

To test this idea experimentally, we incubated WT *E. coli* biofilms as in Figure 1, inoculated them with phages for 24 h, and imaged the system to measure abundance of naïve and lysogenized cells (**Fig 3A)**. We then immediately collected effluent from these microfluidic devices (see Methods) and prepared the contents for imaging with no delay during which cell growth or changes in phage activity could occur. We calculated the relative abundance of lysogens in the liquid effluent and found that indeed the lysogen frequency in the exiting liquid phase is significantly higher than it is in the total biofilm population within the chambers (**Fig 3B,C)**. Specifically, lysogens were 10-fold more likely to be dispersed than the average non-lysogenized naïve host cell in the system. On the other hand, if we isolate only a fraction of the population residing at a cell packing fraction of 0.3 or below, then the lysogens' frequency in this subpopulation becomes indistinguishable from its frequency in the effluent (**S11 Fig).** This observation reinforces the interpretation that the dispersing cells are derived primarily from the outermost, lower-density biofilm regions, which is where the lysogens are most abundant. If we conducted this same experiment after 72 h of phage exposure (as opposed to 24 h from above), the disparity between lysogen frequency in the effluent relative to the total naïve population was even larger. This suggests that the pattern of biased dispersal of lysogens is a persistent feature of the system that strengthens over time as more lysogens are produced by phage-host contact events and growth/division of existing lysogens along the biofilm periphery (**S12 Fig).**

As phage λ carries genes that can modify host outer membrane composition(*72*, *73*), we checked whether λ lysogens are more likely to disperse due to a property conferred by the integrated phage genome itself. To do so we inoculated biofilm chambers with a 1:1 mixture of pre-lysogenized cells and naïve cells and tracked the biovolume of both strains within the chamber and within the effluent. We found no difference in growth rates or dispersal between these two strains when inoculated into chambers at the same time (**S12 Fig)**. These data suggest that in the case when phages are added to an initially non-lysogenized naïve host biofilm, lysogens disperse more frequently than naïve cells not because of a change in biofilm of dispersal physiology among lysogenized cells, but rather due to the spatial arrangement in which lysogens are generated. This interpretation predicts that in Δ*csgBA E. coli* biofilms, which lack the cell-cell packing structure that creates stratified lysogen distributions (Figure 1), there should be no discrepancy between within-biofilm lysogen abundance and liquid effluent lysogen abundance. We tested this idea using our Δ*csgBA E. coli* strain to perform the same experiment in which biofilms were grown for 48 h, inoculated with λ phages for 24 h, and then quantified for lysogen content in the biofilm and effluent phases. As anticipated, we found no difference between the within-biofilm lysogen frequency and the liquid effluent lysogen frequency in this case (**S12 Fig)**. This outcome further supports the interpretation above that WT *E. coli* lysogens preferentially disperse because of the spatially stratified manner in which they occur within a belt of loosely packed host cells on the periphery of biofilms with high interior cell packing.

If lysogens preferentially disperse because they originate in peripheral biofilm regions of low cell density, we would also predict that within larger WT biofilm clusters to which phages have been added, there should be peripheral regions of reduced cell packing from which dispersed lysogens are mostly derived, and therefore in which the within-biofilm lysogen frequency should quantitatively match the liquid effluent lysogen frequency. We assessed this prediction by segmenting the total and the lysogenized cell volumes within WT biofilm exposed to phages for 24 h. We calculated the localized cell-cell packing as was done above and in previous reports(*12*, *13*), and we binned the segmented biomass according to the localized cell packing in the vicinity, seeking to find a cell-packing threshold below which the lysogen frequency in the effluent matched the within-biofilm frequency (**Figure 3B,C**). We performed this analysis different density thresholds and determined that lysogen abundance is accurately reflected by the biofilm composition at cell volume fractions of 0.3 and lower, which can be found in a belt around the biofilm exterior. This region of the biofilms also reflects the median cell packing at which lysogens tend to be located after the initial wave of phage activity along the biofilm exterior (**Figure 1E, Figure 2C)**.

The result that lysogens are especially disposed to disperse from naïve WT biofilms prompted us to consider larger scale patterns of phage and biofilm spatial distribution. We hypothesized that because lysogens are disproportionately likely to depart from biofilms relative to non-lysogenized cells, the new biofilms re-seeded by this dispersal pool downstream from the original population will likely be over-represented for lysogens relative to origin biofilms. We tested this possibility by growing biofilms as above for 48 h, adding phages continuously

for 24 h, sampling effluent these chambers, and inoculating the liquid effluent into fresh microfluidic chambers. This effluent contained mixtures of naïve cells, lysogenized cells, and free λ phages. After a 45 min attachment phase, we incubated these biofilms for 72 h without any additional phage being introduced to the flow devices. After 72 h of growth, the frequency of lysogens in the downstream chambers was significantly higher than what we observed in the original chambers (**Fig 3E**). There was notably high variance in this experimental outcome, which we speculate is due to biological variation in the upstream biofilm population structure and the bottleneck re-colonization events from the effluent samples, which deposited relatively small, noise-prone samples of cells on the glass in downstream biofilm chambers. When we performed this same experiment with our Δ*csgBA* strain of *E. coli*, we saw no difference between the original chambers and downstream chambers at equivalent time points, again consistent with all of the analyses above (**Fig 3E**).

Altogether, our data suggest that the natural spatial constraints of biofilm cell group architecture led to a repeatable pattern of lysogen generation and expansion when naïve biofilms are exposed to a pulse of temperate phages. Lysogens tend to be concentrated in the periphery of established, density packed biofilm clusters and equilibrate at ~10% of total population, because λ phages only rarely diffuse to areas past a characteristic cell packing threshold and are also neutralized by previously lysogenized cells. Concentrated on the periphery of biofilm clusters, where cell packing tends to be lower and is decreased further by lytic cycle phage activity, lysogens are inherently prone to disperse and become over-represented in the pool of planktonic cells exiting the system (**S13 Fig**). This leads to their further overrepresentation in new biofilm populations seeded downstream of the biofilm from which they originated. The overall nature of temperate phage propagation by host lysis and lysogenization has the effect of increasing the efficiency of spatial spread of lysogenized cells relative to other phage life history strategies. Lysogens tend to be created amidst a wave of lytic activity that decreases local cell packing and likely increases dispersal propensity, leading to new biofilms that rapidly become populated by high numbers of lysogens at distal locations.

Temperate phages rapidly increase in frequency during biofilm dispersal

Because temperate phages can spread through biofilms as either lysogenized cells or as active phage particles, we were interested in how the unique life history strategy of temperate phages influences their spread in biofilms through space and time. To examine how a phage's ability to lysogenize hosts influences propagation through a biofilm in finer detail, we first performed experiments in which *E. coli* biofilms were grown as in Figure 1, and then inoculated these biofilms with either phage λ, λΔ*cI*, or T7 phages in separate experimental replicates at equal phage titers. T7 is an obligately lytic phage that must kill its host in order to propagate. This strain of T7 contains a transcriptional fusion encoding *sfGFP*, which causes host cells to fluoresce green prior to lysis (*31*). We constructed the λΔ*cI* strain by replacing the cI locus encoding Repressor with a truncated nonfunctional copy; this phage retains the mTurquoise2 capsid decoration protein fusion, such that phage particles can still be tracked. But without a functional copy of cI for Repressor synthesis, λΔ*cI* can only propagate by lytic infection (**S14 Fig**).

We monitored phage propagation in biofilm chambers exposed to phages continuously for 7 h, then removed phages from media flowing into the chambers and returned sterile medium flow to them for 3 h to remove any phages that were not physically associated with the biofilm-dwelling host population. We then connected the effluent lines of these microfluidic devices to new ('downstream') devices and allowed cells and phages to colonize the new chambers for 2 h; finally, new influent tubing was connected to the down-stream chambers to introduce sterile media for an additional 96 h. We used infected cell biovolume as our metric for phage spread and propagation in our biofilm chambers, where cells can be determined to be infected if they are undergoing the lytic cell fate or if they are lysogenized. Assessing phage fitness using infected cell counts, including lysogens, has been established as the most robust metric for studying phage population dynamics in recent theory work (*74–76*).

In the first 7 h of exposure to phage T7, we see the highest accumulation of infected cells relatively early, just 2 h after phages are inoculated into the biofilms (**Fig 4A, B)**. This is followed by a rapid decrease in infected cells, as the T7 phages have killed and lysed most of the cells in the chambers (**Fig 4A, B)**. When we conduct

this experiment with λ or λΔ*cI* phages, we observe qualitatively different population dynamics than with T7. Rather than an early peak followed by subsequent decrease in infected cell biovolume, we see a slow increase in infected cell numbers, contributed to by both lytic and lysogenic cell fates for WT λ, and only lytic cell fates for λΔ*cI*. If we instead measure the infected cell frequency as a function of the total population, we observe T7 phages reach their highest frequency within 4 h of inoculation in the original chamber, followed by a decrease as cells continue to lyse and they exhaust their prey population. Infected cell frequency of λ and λΔ*cI* phages remain low during the 7 h in the original chamber, which is consistent with the above findings in Figure 1 and Figure 2.

To follow phage and host dynamics over larger spatial scales, we repeated the downstream chamber recolonization experiment in which effluent from upstream chambers was used to inoculate new, sterile chambers. For phage T7, we occasionally found no cells – infected or uninfected – in downstream chambers (**Fig 4E)**. More frequently, we found a small population of *E. coli* cells that had colonized the surface, with a small proportion of these cells actively infected with T7. As a result, the biovolume of infected cells for T7 is lower than λ, and infected cells also make up a low frequency of the total population (**Fig 4F)**. In the downstream chambers infected with λ phages, we observe an increase in infected cell biovolume, primarily driven by lysogenized cells continuing to divide and populate the new biofilm (**Fig 4E**). The active phage particles in this system also continue to lyse and lysogenize uninfected cells, further contributing to the increase in biovolume of infected cells, as well as the high infected cell frequency (**Fig 4F**). For downstream chambers of λΔ*cI*, we observed a lower infected cell frequency than for λ, but a higher biovolume of infected cells than for T7 (**Fig 4E, F**), which we attribute to T7 being a more virulent phage that more rapidly kills host cells relative to bacterial growth and division. So, in the original chamber where phages were added continuously for 7 h, we observed T7 accumulating higher fitness in virocell terms than λ phages. However, in the downstream chambers, we see the opposite effect, where temperate λ phages accumulate higher biovolume of infected cells, and infected cells dominate the population over extended time scales. This outcome indicates that virulent and temperate phage strategies are differentially suited to propagation on short time and small spatial scales (for quickly replicating virulent phages), versus propagation over longer time and larger spatial scales (for temperate phages).

Discussion

Live, high-resolution imaging of bacteria and phages dwelling in biofilms provides unique and crucial insight into the ecology of microbes on the spatial scale at which their behavior directly manifests. Here we tracked the spatial propagation of temperate phage λ in sensitive *E. coli* biofilms, finding repeatable patterns in the localization of phages and lysogens along the periphery of biofilm cell groups. This localization leads to preferential dispersal of lysogenized cells to new locations, which in turn confers several unique benefits to the temperate phage strategy in biofilm populations. Due to the spatial arrangement of newly created lysogens in wildtype biofilms, we find that lysogens are significantly over-represented in the effluent dispersal pool that departs from the stationary host population. Because the temperate phage strategy predisposes itself to dispersal from biofilms of origin, their fitness is far greater over longer time scales and, most pertinently, over larger spatial scales on which dispersed cells from one biofilm population colonize new locations to produce new downstream biofilms.

This study provides a first look into the complex interactions of temperate phages and their host bacteria in a biofilm context, examining them at the cellular spatial scale on which microbial phenotypes directly manifest. For simplicity within this system, we explored a single species of bacteria and a single strain of phage, however further studies can expand on these results by increasing ecological realism in terms of species richness within bacterial biofilm communities, as well as greater diversity among the phages introduced to these communities. While our lysogenized *E. coli* is not distinguishable from parental non-lysogens in terms of biofilm production, many temperate phages change host behavior by introducing novel functions to them via lysogeny, including alterations to metabolism and extracellular product secretion(*23*, *25*). How the traits introduced by prophages alter biofilm community dynamics of their hosts remains a largely unexplored topic and a promising direction for future work.

Acknowledgements

We are grateful to Robert Cramer, Yuncong Geng, Ido Golding, Thu Vu Phuc Nguyen, and Stephen Winans and for feedback on earlier versions of this manuscript, and to members of the Nadell Lab and microbiology community at Dartmouth for feedback on the project. The authors also extend thanks to Thu Vu Phuc Nguyen and Siân Owen for their advice and the pSIM5 plasmid, which were critical for engineering the λΔ*cI* strain used in this study.

Additional Information

J.B.W. was supported by a NIH T32 training grant (award number AI007519), John H. Copenhaver Jr. Fellowship, and a GAANN Fellowship. BioMT is supported by NIGMS COBRE award P20-GM113132. CDN is supported by the Human Frontier Science Program (award number RGY0077/2020), the Simons Foundation (award number 826672), NSF IOS grant 2017879, and NIGMS grant 1R35GM151158-01.

Methods

Strains

E. coli strains used in this project were all AR3110 derivatives. AR3110 was derived from the K-12 strain W3110, which does not produce cellulose because of a polar stop codon mutation in *bcsQ*. This stop codon mutation was corrected in AR3110 to yield a strain that produces cellulose, thus restoring this *E. coli* strain to "wild-type" biofilm formation secreting cellulose and curli protein. Like other K-12 derivatives, AR3110 is susceptible to both T7 phages and λ phages. Strains of AR3110 were engineered via lambda red recombination or through SacB allelic exchange. Briefly, primers encoding regions of homology to the flanking regions of the gene of interest were used to amplify the Kan^R resistance cassette flanked by FRT sites. For creating fluorescent strains, these resistance cassettes were fused to fluorescent protein constructs via SOE PCR. These PCR products were used to knock out genes of interest and selected for with the resistance cassette. FRT sites were used to flip-out the resistance cassette if desired. SacB allelic exchange was performed by constructing plasmids containing regions of homology to flanking regions and gene insertion, SacB, and a selective resistance marker. Plasmids were transformed into *E. coli* through electroporation and screened for kanamycin resistance, then counter-selected on sucrose plates to remove the antibiotic marker and native allele. Recombinant T7 phages were produced previously using T7select415-1 phage display. Recombinant λ phages were produced by infecting λD*am* cI_{857} *bor::KanR* phages on LE392 (permissive host) with the pBR322-λD-mTurquoise2/mNeongreen-E plasmid to allow for recombination, and further selection for fluorescent plaques. λΔ*cI* was created via lambda-red recombination that introduced a truncated nonfunctional copy of *cI* followed by screening for clear plaques(*77*). Newly generated strains for this paper will be available upon request.

Microfluidic flow device fabrication

Microfluidic devices were produced by casting poly-dimethysiloxane (PDMS; Dow Chemical Company, SYLGARD 184, cat. # 04019862) onto premade device molds (a schematic for this can be found in **S1 Fig)**. The resulting PDMS blocks were cut out of the molds, hole-punched for inlet and outlet channels, and then bonded to #1.5 glass coverslips using plasma cleaning preparation of the PDMS and glass coverslips (Azer Scientific, cat. # 1152260). Between the inlet and outlet port areas, the internal space of the chambers in which biofilms were incubated measured 5,000 μm × 500 μm × 70 μm (LxWxH). Segments of inlet tubing (Cole Parmer PTFE #30, cat. # 06417–11) attached to 27Gx1/2 needles (BD Precision, cat. # 305109) on 1 milliliter syringes (Brandzig, cat. #CMD2583) were plumbed into chamber inlets, and the syringes were pushed by Harvard Apparatus Pico Plus Elite syringe pumps (Harvard Apparatus, cat. # 70–4506). Tubing from chamber outlet channels was fed to effluent waste collection.

Biofilm culture conditions

Overnight cultures of *E. coli* were inoculated into the microfluidic chambers. After a 45-min incubation period without flow to allow for surface attachment, M9 minimal media with 0.5% maltose continuously flowed into the device at a rate of 0.1 μL/min. For the immunostaining of curli, our AR3110 strain harboring a translational 6xHis tag fused to csgA, which encodes the monomer for curli production, was stained with Anti-6X His Epitope Tag (Rabbit) antibody conjugated to Dylight 405 (Rockland Immunochemicals, cat. # 600-446-382) added to the media at a concentration of 0.1 μg/mL continuously for the entirety of the experiment. Prior work has shown that addition of the 6xHis tag to CsgA does not interrupt its function by any measures tested. All experiments were carried out at room temperature.

Phage propagation and introduction to biofilms

λ phages were produced by growing lysogenic *E. coli* to an OD_{600} = 0.2 in M9 minimal media with 0.5% maltose, then heat shocked at 42˚C for 20 min, and then incubated at 37˚C until visible lysis occurred. T7 phages were produced by growing sensitive E. coli to OD_{600} = 0.4 in M9 minimal media with 0.5% maltose, before adding an aliquot of T7 phage and incubating until the bacterial cultures were cleared. Phages were quantified using standard plaquing techniques and back-diluted to 10^4/μL in M9 with 0.5% maltose. To visualize phage infection, we used a previously constructed T7 strain that induces sfGFP production by the host prior to lysis. For experiments with short phage exposure, phages were continuously introduced for 24 h. For experiments with

extended phage exposure (Fig 2), phages were continuously added for 120 h. For the nascent biofilm phage exposures investigating spatial patterning in the absence of established biofilms, phages were introduced into the chamber immediately following the initial attachment step.

Biofilm dispersal and detection of *de novo* λ-resistance mutants from biofilm culture

E. coli biofilms grown for 48 h and then treated with λΔ*cI* phages for 24 h were dispersed from the biofilm by removing the tubing from the microfluidic device and vigorously pipetting 100 μL of M9 media and air bubbles back and forth between the inlet and outlet ports. This was done to ensure maximal removal of all cells in the chamber in order to capture accurate measurements of total *E. coli* and any de novo λ-resistant *E. coli*. To determine cell viability and phage sensitivity, this 100 μL volume containing dispersed biofilm cells was serially diluted and plated on LB plates for total *E. coli* counts and, in parallel, on LB plates saturated with λΔ*cI* phages to determine *de novo* λ-resistant counts.

Phage adsorption assay

Bacterial cultures of uninfected *E. coli*, lysogenic *E. coli*, and *E. coli ΔlamB* were grown and back-diluted to an OD_{600} = 0.2 in λ medium. λ phages were added to a final concentration of 5×10^3 phages per μL. Cultures were incubated at 30˚C on an orbital shaking platform, and 200 μL aliquots were taken every 25 min, passed through a 0.2-μm filter, and stored on ice until the end of the experiment. The filtration step served to exclude any bacterial cells, and any phages that were attached to them, allowing us to measure free phages remaining in the liquid medium. Flowthrough samples were then serially diluted and plated for PFUs.

Phage adsorption and *E. coli* population dynamics assay

Sensitive *E. coli* was grown and back-diluted to an OD_{600} = 0.2 in λ medium. λ phages were added to a final concentration of 5×10^3 phages per μL. Cultures were again incubated at 30˚C on an orbital shaking platform, and 200 μL aliquots were taken every 25 min, passed through a 0.2-μm filter, and stored on ice until the end of the experiment. Another 20μL aliquot was taken and directly added to a dilution series in a 96-well plate. To avoid *E. coli* amplification after sampling, these samples were immediately serially diluted and plated for CFUs. After all of the samples were collected, flowthrough phage samples were serially diluted for PFUs.

Biofilm effluent and recolonization assay

Biofilms were incubated for 48 h without phage exposure, treated with phage for 24 h, and then imaged. We then shortened the effluent tubing to allow for effective collection, and increased flow to 1 μL/min to collect 10uL of media. A portion of this sample was imaged under an agar pad to determine lysogen abundance. Another portion of this sample was used to inoculate new microfluidic devices, incubated without the addition of exogenous phages. These new microfluidic devices were tracked through time.

Microscopy and image analysis

All imaging was performed using a Zeiss 980 line-scanning confocal microscope, using a 40x/1.2 N.A. water objective or a 10x/.4 N.A. water objective. The 6xHis Tag Antibody Dylight 405 that was used to stain 6xHis-tagged curli polymers was excited with a 405 laser line. The mTurquoise2 protein that λ and λΔ*cI* phage capsid produces was excited with the 458 laser line. The sfGFP protein produced by the T7 infection reporter construct was excited with a 488 laser line. The mKO2 protein that lysogenic *E. coli* expresses constitutively was excited with a 543 laser line. The mKate2 protein that WT *E. coli* and Δ*csgBA E. coli* express constitutively was excited with a 594 laser line (in separate experiments). If one image was not sufficient in order to capture the variation seen within a given microfluidic device, multiple independent locations were chosen within each biofilm chamber and averaged to give 1 measurement for a given chamber in the case of whole-biofilm measurements. Prior to export, images were processed by constrained iterative deconvolution in ZEN blue.

Replication, quantification, and statistics

Replication is reported for each experiment individually in the legends of all of the figures. The reported n for each figure panel refers to biological replicates. One biological replicate was defined as the averaged outcome for measurements across a single microfluidic flow chamber inoculated from independent overnight culture

preparations. Biological replicates for the core experiments in the study were performed across 3 weeks with independent microfluidic chambers. Technical replicates were separate z-stacks captured at randomized locations throughout a given flow chamber; measurements from these technical replicates were averaged to calculate the value for the biological replicate corresponding to that flow chamber. All biofilm image quantification was performed within the BiofilmQ framework. For 3D grid-based measurements detailing microscale architecture, segmented microbial volumes were divided into a 3D grid with each node 0.72 µm on a side. Joint neighborhood cell packing measurements merged the biovolume of all bacteria within a sample and calculated the local biovolume fraction within 6 µm of each segmented bacterial volume within each grid cube. Mann–Whitney U tests with the Bonferroni correction were used for pairwise comparisons. We chose nonparametric comparison tests because they are relatively conservative and because the assumptions required for parametric tests could not consistently be assessed for our data.

Table 1. Reagents, products, and software used in this study

Strain	**Relevant markers/Genotype**	**Source**
Bacteria		
CNE859	AR3110, mTurquoise2/mKO2 λ, 6x-*His* csgA	This study
CNE863	AR3110, *Lac::mKatex2*, *6x-His csgA*, AmpR-gpD plasmid	This study
CNE866	AR3110, mTurquoise2/mKO2 λ, 6x-*His* csgA, AmpR-gpD	This study
CNE869	AR3110, *Lac::mKatex2*, *ΔcsgBA*::KanR, AmpR-gpD plasmid	This study
CNE881	AR3110, Δ*lamB::KanR, mKate2*	This study
CNE907	AR3110, Δ*lamB, sfGFP, ΔcsgBA*::KanR	This study
CNE908	AR3110, Δ*csgBA::KanR*, mKate2, mTurquoise2/mKO2 λ, AmpR-gpD plasmid	This study
CNE909	AR3110, mTurquoise2/mKO2 λ, AmpR-gpD plasmid, pSIM5-tetR	This study
Phages		
CNX11	T7 with sfGFP under control of phi 10 promoter	(*31*)
λLZ1367	*λD-mTurquoise2* cI_{857}*-mKO2 bor::CmR*	(*65*)
CNX20	*λD-mTurquoise2,* truncated $cI_{1\text{-}17::223\text{-}239}$ *, bor::CmR*	This study
Chemicals and reagents	**Source**	**Product number**
Kanamycin	Millipore-Sigma	cat.#60615
MEM Vitamin Solutions	Millipore-Sigma	cat. #M6895
Alexa Fluor™ 633 NHS Ester	ThermoFisher Scientific	cat. # A20005
Anti-6X His Epitope Tag (Rabbit) antibody conjugated to Dylight 405	Rockland Immunochemicals	cat. # 600-446-382
Poly-dimethysiloxane (PDMS)	Dow Chemical Company; SYLGARD 184	cat. # 04019862
#1.5 glass coverslips	Azer Scientific	cat. # 1152260
Inlet tubing	Cole Parmer	cat. # 06417-11
27Gx1/2 needles	BD Precision	cat. # 30510
1mL syringes	Brandzig	cat. #CMD2583
Harvard Apparatus Pico Plus Elite syringe pumps	Harvard Apparatus	cat. # 70-4506
Software and Algorithms	**Source**	**Version**
Zen Black	Zeiss	v14.0.0.0
Zen Blue	Zeiss	v3.4.91.00000
MATLAB	MathWorks	vR2021a
Paraview	Kitware	v5.9.1
Prism	GraphPad	v9.4.1
BiofilmQ	(61)	v0.2.2

References

1. J. Krause, P. of F. B. and E. J. Krause, G. D. Ruxton, G. Ruxton, I. G. Ruxton, *Living in Groups* (OUP Oxford, 2002).

2. S. Marras, S. S. Killen, J. Lindström, D. J. McKenzie, J. F. Steffensen, P. Domenici, Fish swimming in schools save energy regardless of their spatial position. *Behav. Ecol. Sociobiol.* **69**, 219–226 (2015).

3. L. M. Southern, T. Deschner, S. Pika, Lethal coalitionary attacks of chimpanzees (Pan troglodytes troglodytes) on gorillas (Gorilla gorilla gorilla) in the wild. *Sci. Rep.* **11**, 14673 (2021).

4. I. D. Couzin, J. Krause, R. James, G. D. Ruxton, N. R. Franks, Collective memory and spatial sorting in animal groups. *J. Theor. Biol.* **218**, 1–11 (2002).

5. A. Roussi, Why gigantic locust swarms are challenging governments and researchers. *Nature* **579**, 330 (2020).

6. A. F. Miranda, N. Ramkumar, C. Andriotis, T. Höltkemeier, A. Yasmin, S. Rochfort, D. Wlodkowic, P. Morrison, F. Roddick, G. Spangenberg, B. Lal, S. Subudhi, A. Mouradov, Applications of microalgal biofilms for wastewater treatment and bioenergy production. *Biotechnol. Biofuels* **10**, 120 (2017).

7. H.-C. Flemming, J. Wingender, U. Szewzyk, P. Steinberg, S. A. Rice, S. Kjelleberg, Biofilms: an emergent form of bacterial life. *Nat. Rev. Microbiol.* **14**, 563–575 (2016).

8. C. D. Nadell, J. B. Xavier, K. R. Foster, The sociobiology of biofilms. *FEMS Microbiol. Rev.* **33**, 206–224 (2009).

9. C. D. Nadell, K. Drescher, N. S. Wingreen, B. L. Bassler, Extracellular matrix structure governs invasion resistance in bacterial biofilms. *ISME J.* **9**, 1700–1709 (2015).

10. M. E. Hibbing, C. Fuqua, M. R. Parsek, S. B. Peterson, Bacterial competition: surviving and thriving in the microbial jungle. *Nat. Rev. Microbiol.* **8**, 15–25 (2010).

11. D. P. Pires, L. D. R. Melo, J. Azeredo, Understanding the Complex Phage-Host Interactions in Biofilm Communities. *Annu. Rev. Virol.* **8**, 73–94 (2021).

12. J. B. Winans, B. R. Wucher, C. D. Nadell, Multispecies biofilm architecture determines bacterial exposure to phages. *PLOS Biol.* **20**, e3001913 (2022).

13. B. R. Wucher, J. B. Winans, M. Elsayed, D. E. Kadouri, C. D. Nadell, Breakdown of clonal cooperative architecture in multispecies biofilms and the spatial ecology of predation. *Proc. Natl. Acad. Sci. U. S. A.* **120**, e2212650120 (2023).

14. B. R. Wucher, M. Elsayed, J. S. Adelman, D. E. Kadouri, C. D. Nadell, Bacterial predation transforms the landscape and community assembly of biofilms. *Curr. Biol.* **31**, 2643-2651.e3 (2021).

15. J. Azeredo, N. F. Azevedo, R. Briandet, N. Cerca, T. Coenye, A. R. Costa, M. Desvaux, G. Di Bonaventura, M. Hébraud, Z. Jaglic, M. Kačániová, S. Knøchel, A. Lourenço, F. Mergulhão, R. L. Meyer, G. Nychas, M. Simões, O. Tresse, C. Sternberg, Critical review on biofilm methods. *Crit. Rev. Microbiol.* **43**, 313–351 (2017).

16. H. G. Hampton, B. N. J. Watson, P. C. Fineran, The arms race between bacteria and their phage foes. *Nature* **577**, 327–336 (2020).

17. S. R. Casjens, R. W. Hendrix, Bacteriophage lambda: early pioneer and still relevant. *Virology* **0**, 310–330 (2015).

18. E. Pfeifer, R. A. Bonnin, E. P. C. Rocha, Phage-Plasmids Spread Antibiotic Resistance Genes through Infection and Lysogenic Conversion. *mBio* **13**, e01851-22 (2022).

19. M. K. Waldor, J. J. Mekalanos, Lysogenic conversion by a filamentous phage encoding cholera toxin. *Science* **272**, 1910–1914 (1996).

20. Y. Sakaguchi, T. Hayashi, K. Kurokawa, K. Nakayama, K. Oshima, Y. Fujinaga, M. Ohnishi, E. Ohtsubo, M. Hattori, K. Oguma, The genome sequence of Clostridium botulinum type C neurotoxin-converting phage and the molecular mechanisms of unstable lysogeny. *Proc. Natl. Acad. Sci. U. S. A.* **102**, 17472–17477 (2005).

21. P. Blanco-Picazo, S. Morales-Cortes, M. D. Ramos-Barbero, C. García-Aljaro, L. Rodríguez-Rubio, M. Muniesa, Dominance of phage particles carrying antibiotic resistance genes in the viromes of retail food sources. *ISME J.*, doi: 10.1038/s41396-022-01338-0 (2022).

22. R. C. Molina-Quiroz, T. N. Dalia, A. Camilli, A. B. Dalia, C. A. Silva-Valenzuela, Prophage-Dependent Neighbor Predation Fosters Horizontal Gene Transfer by Natural Transformation. *mSphere* **5**, e00975-20 (2020).

23. K. Gozzi, N. T. Tran, J. W. Modell, T. B. Le, M. T. Laub, Prophage-like gene transfer agents promote Caulobacter crescentus survival and DNA repair during stationary phase. *PLoS Biol.* **20**, e3001790 (2022).

24. B. Koskella, M. A. Brockhurst, Bacteria–phage coevolution as a driver of ecological and evolutionary processes in microbial communities. *FEMS Microbiol. Rev.* **38**, 916–931 (2014).

25. A. Krüger, P. M. A. Lucchesi, Shiga toxins and stx phages: highly diverse entities. *Microbiol. Read. Engl.* **161**, 451–462 (2015).

26. E. M. Lederberg, J. Lederberg, Genetic Studies of Lysogenicity in Escherichia Coli. *Genetics* **38**, 51–64 (1953).

27. M. Ptashne, *A Genetic Switch, Third Edition: Phage Lambda Revisited* (Cold Spring Harbor Laboratory Press, Cold Spring Harbor, N.Y, 3rd edition., 2004).

28. C. Howard-Varona, K. R. Hargreaves, S. T. Abedon, M. B. Sullivan, Lysogeny in nature: mechanisms, impact and ecology of temperate phages. *ISME J.* **11**, 1511–1520 (2017).

29. F. St-Pierre, D. Endy, Determination of cell fate selection during phage lambda infection. *Proc. Natl. Acad. Sci. U. S. A.* **105**, 20705–20710 (2008).

30. D. Ping, T. Wang, D. T. Fraebel, S. Maslov, K. Sneppen, S. Kuehn, Hitchhiking, collapse, and contingency in phage infections of migrating bacterial populations. *ISME J.* **14**, 2007–2018 (2020).

31. L. Vidakovic, P. K. Singh, R. Hartmann, C. D. Nadell, K. Drescher, Dynamic biofilm architecture confers individual and collective mechanisms of viral protection. *Nat. Microbiol.* **3**, 26–31 (2018).

32. S. E. Darch, K. N. Kragh, E. A. Abbott, T. Bjarnsholt, J. J. Bull, M. Whiteley, Phage Inhibit Pathogen Dissemination by Targeting Bacterial Migrants in a Chronic Infection Model. *mBio* **8**, e00240-17 (2017).

33. V. Dunsing, T. Irmscher, S. Barbirz, S. Chiantia, Purely Polysaccharide-Based Biofilm Matrix Provides Size-Selective Diffusion Barriers for Nanoparticles and Bacteriophages. *Biomacromolecules* **20**, 3842–3854 (2019).

34. F. Díaz-Pascual, R. Hartmann, M. Lempp, L. Vidakovic, B. Song, H. Jeckel, K. M. Thormann, F. H. Yildiz, J. Dunkel, H. Link, C. D. Nadell, K. Drescher, Breakdown of Vibrio cholerae biofilm architecture induced by antibiotics disrupts community barrier function. *Nat. Microbiol.* **4**, 2136–2145 (2019).

35. R. S. Eriksen, F. Larsen, S. L. Svenningsen, K. Sneppen, N. Mitarai, The dynamics of phage predation on a microcolony. *Biophys. J.* (2023).

36. M. C. Bond, L. Vidakovic, P. K. Singh, K. Drescher, C. D. Nadell, Matrix-trapped viruses can prevent invasion of bacterial biofilms by colonizing cells. *eLife* **10**, e65355 (2021).

37. E. L. Simmons, M. C. Bond, B. Koskella, K. Drescher, V. Bucci, C. D. Nadell, Biofilm Structure Promotes Coexistence of Phage-Resistant and Phage-Susceptible Bacteria. *mSystems* **5**, e00877-19 (2020).

38. E. L. Simmons, K. Drescher, C. D. Nadell, V. Bucci, Phage mobility is a core determinant of phage–bacteria coexistence in biofilms. *ISME J.* **12**, 531–543 (2018).

39. B. Andrews, S. Fields, Balance between promiscuity and specificity in phage λ host range. *ISME J.* **15**, 2195–2205 (2021).

40. S. O'Brien, R. Kümmerli, S. Paterson, C. Winstanley, M. A. Brockhurst, Transposable temperate phages promote the evolution of divergent social strategies in Pseudomonas aeruginosa populations. *Proc. R. Soc. B Biol. Sci.* **286**, 20191794 (2019).

41. P. Moons, D. Faster, A. Aertsen, Lysogenic Conversion and Phage Resistance Development in Phage Exposed Escherichia coli Biofilms. *Viruses* **5**, 150–161 (2013).

42. S. G. Sutcliffe, A. Reyes, C. F. Maurice, Bacteriophages playing nice: Lysogenic bacteriophage replication stable in the human gut microbiota. *iScience* **26**, 106007 (2023).

43. J. E. Silpe, B. L. Bassler, A host-produced quorum-sensing autoinducer controls a phage lysis-lysogeny decision. *Cell* **176**, 268–280 (2019).

44. D. Dar, N. Dar, L. Cai, D. K. Newman, Spatial transcriptomics of planktonic and sessile bacterial populations at single-cell resolution. *Science* **373**, eabi4882 (2021).

45. D. O. Serra, A. M. Richter, R. Hengge, Cellulose as an Architectural Element in Spatially Structured Escherichia coli Biofilms. *J. Bacteriol.* **195**, 5540–5554 (2013).

46. A. M. Richter, A. Possling, N. Malysheva, K. P. Yousef, S. Herbst, M. von Kleist, R. Hengge, Local c-di-GMP Signaling in the Control of Synthesis of the E. coli Biofilm Exopolysaccharide pEtN-Cellulose. *J. Mol. Biol.* **432**, 4576–4595 (2020).

47. M. R. Chapman, L. S. Robinson, J. S. Pinkner, R. Roth, J. Heuser, M. Hammar, S. Normark, S. J. Hultgren, Role of Escherichia coli Curli Operons in Directing Amyloid Fiber Formation. *Science* **295**, 851–855 (2002).

48. D. A. Hufnagel, W. H. Depas, M. R. Chapman, The Biology of the Escherichia coli Extracellular Matrix. *Microbiol. Spectr.* **3**, 10.1128/microbiolspec.mb-0014–2014 (2015).

49. T. Wang, P. Shen, Y. He, Y. Zhang, J. Liu, Spatial transcriptome uncovers rich coordination of metabolism in E. coli K12 biofilm. *Nat. Chem. Biol.*, 1–11 (2023).

50. C. Beloin, A. Roux, J.-M. Ghigo, Escherichia coli biofilms. *Curr. Top. Microbiol. Immunol.* **322**, 249–289 (2008).

51. R. Ziege, A.-M. Tsirigoni, B. Large, D. O. Serra, K. G. Blank, R. Hengge, P. Fratzl, C. M. Bidan, Adaptation of Escherichia coli Biofilm Growth, Morphology, and Mechanical Properties to Substrate Water Content. *ACS Biomater. Sci. Eng.* **7**, 5315–5325 (2021).

52. D. O. Serra, R. Hengge, Bacterial Multicellularity: The Biology of *Escherichia coli* Building Large-Scale Biofilm Communities. *Annu. Rev. Microbiol.* **75**, 269–290 (2021).

53. T. V. P. Nguyen, Y. Wu, T. Yao, J. T. Trinh, L. Zeng, Y. R. Chemla, I. Golding, Co-infecting phages impede each other's entry into the cell. bioRxiv [Preprint] (2023). https://doi.org/10.1101/2023.06.05.543643.

54. T. Yao, S. Coleman, T. V. P. Nguyen, I. Golding, O. A. Igoshin, Bacteriophage self-counting in the presence of viral replication. *Proc. Natl. Acad. Sci. U. S. A.* **118**, e2104163118 (2021).

55. P. Kourilsky, Lysogenization by bacteriophage lambda. I. Multiple infection and the lysogenic response. *Mol. Gen. Genet. MGG* **122**, 183–195 (1973).

56. D. J. Mackay, V. C. Bode, Events in lambda injection between phage adsorption and DNA entry. *Virology* **72**, 154–166 (1976).

57. L. Letellier, L. Plançon, M. Bonhivers, P. Boulanger, Phage DNA transport across membranes. *Res. Microbiol.* **150**, 499–505 (1999).

58. P. Kourilsky, A. Knapp, Lysogenization by bacteriophage lambda: III. - Multiplicity dependent phenomena occuring upon infection by lambda. *Biochimie* **56**, 1517–1523 (1975).

59. J. R. Meyer, D. T. Dobias, J. S. Weitz, J. E. Barrick, R. T. Quick, R. E. Lenski, Repeatability and Contingency in the Evolution of a Key Innovation in Phage Lambda. *Science* **335**, 428–432 (2012).

60. J. M. Borin, J. J. Lee, A. Lucia-Sanz, K. R. Gerbino, J. S. Weitz, J. R. Meyer, Rapid bacteria-phage coevolution drives the emergence of multiscale networks. *Science* **382**, 674–678 (2023).

61. S. Casjens, DNA packaging by the lambdoid phages – From pure beginnings to applications in genetic engineering. *BioEssays* **16**, 847–851 (1994).

62. R. W. Hendrix, Bacteriophages: Evolution of the Majority. *Theor. Popul. Biol.* **61**, 471–480 (2002).

63. S. R. Casjens, R. W. Hendrix, Locations and amounts of major structural proteins in bacteriophage lambda. *J. Mol. Biol.* **88**, 535–545 (1974).

64. G. C. Lander, A. Evilevitch, M. Jeembaeva, C. S. Potter, B. Carragher, J. E. Johnson, Bacteriophage lambda stabilization by auxiliary protein gpD: timing, location, and mechanism of attachment determined by cryoEM. *Struct. Lond. Engl. 1993* **16**, 1399 (2008).

65. J. T. Trinh, T. Székely, Q. Shao, G. Balázsi, L. Zeng, Cell fate decisions emerge as phages cooperate or compete inside their host. *Nat. Commun.* **8**, 14341 (2017).

66. J. T. Trinh, Q. Shao, J. Guan, L. Zeng, Emerging heterogeneous compartments by viruses in single bacterial cells. *Nat. Commun.* **11**, 3813 (2020).

67. L. Zeng, S. O. Skinner, C. Zong, J. Sippy, M. Feiss, I. Golding, Decision Making at a Subcellular Level Determines the Outcome of Bacteriophage Infection. *Cell* **141**, 682–691 (2010).

68. P. C. M. Fogg, H. E. Allison, J. R. Saunders, A. J. McCarthy, Bacteriophage Lambda: a Paradigm Revisited. *J. Virol.* **84**, 6876–6879 (2010).

69. K. Ranade, A. R. Poteete, Superinfection exclusion (sieB) genes of bacteriophages P22 and lambda. *J. Bacteriol.* **175**, 4712–4718 (1993).

70. S. Brown, N. Mitarai, K. Sneppen, Protection of bacteriophage-sensitive *Escherichia coli* by lysogens. *Proc. Natl. Acad. Sci.* **119**, e2106005119 (2022).

71. J. Bondy-Denomy, J. Qian, E. R. Westra, A. Buckling, D. S. Guttman, A. R. Davidson, K. L. Maxwell, Prophages mediate defense against phage infection through diverse mechanisms. *ISME J.* **10**, 2854–2866 (2016).

72. S. Vica Pacheco, O. García González, G. L. Paniagua Contreras, The lom gene of bacteriophage lambda is involved in Escherichia coli K12 adhesion to human buccal epithelial cells. *FEMS Microbiol. Lett.* **156**, 129–132 (1997).

710 73. J. J. Barondess, J. Beckwith, bor gene of phage lambda, involved in serum resistance, encodes a widely conserved outer membrane lipoprotein. *J. Bacteriol.* **177**, 1247–1253 (1995).

74. G. Li, M. H. Cortez, J. Dushoff, J. S. Weitz, When to be temperate: on the fitness benefits of lysis vs. lysogeny. *Virus Evol.* **6**, veaa042 (2020).

75. J. S. Weitz, G. Li, H. Gulbudak, M. H. Cortez, R. J. Whitaker, Viral invasion fitness across a continuum from lysis to
715 latency†. *Virus Evol.* **5**, vez006 (2019).

76. S. Shivam, G. Li, A. Lucia-Sanz, J. S. Weitz, Timescales modulate optimal lysis–lysogeny decision switches and near-term phage reproduction. *Virus Evol.* **8**, veac037 (2022).

77. L. Thomason, D. L. Court, M. Bubunenko, N. Costantino, H. Wilson, S. Datta, A. Oppenheim, Recombineering: Genetic Engineering in Bacteria Using Homologous Recombination. *Curr. Protoc. Mol. Biol.* **78**, 1.16.1-1.16.24
720 (2007).

Figures

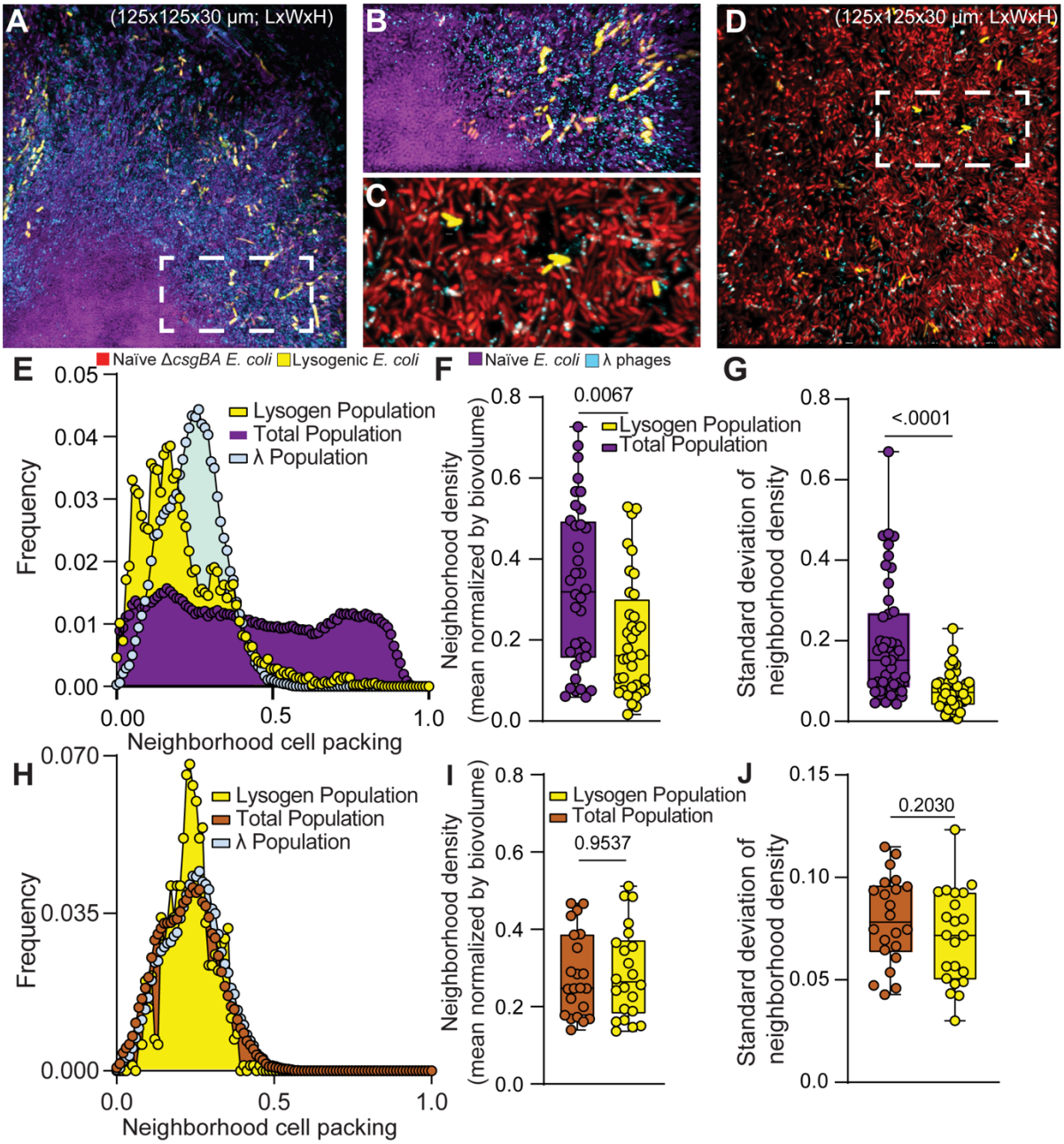

Figure 1. (A, B) *E. coli* (purple) invaded with λ phages (turquoise) for 24 h, with some cells becoming lysogenic (yellow) with a specific spatial pattern. (B) is a magnified image of the box dashed white box in (A). (C, D) Δ*csgBA E. coli* (red) invaded with λ phages (turquoise) for 24 h, with some cells becoming lysogenic (yellow) with no detectable spatial patterning of initial lysogeny events. (C) is a magnified image of the box dashed white box in (D). (E) The frequency distribution of the neighborhood cell packing for the lysogen and total populations. (F) The mean neighborhood density of the total population compared to the newly lysogenized population, normalized by biovolume (n=36). (F) The standard deviation of neighborhood density (n=45). (H) Frequency distribution of the neighborhood cell packing for the lysogen and total populations. (I) The mean neighborhood density normalized by biovolume (n=22). (J) The standard deviation of neighborhood density (n=22). Statistical tests shown are Mann-Whitney U tests to account for unpaired, non-normally distributed, data collected.

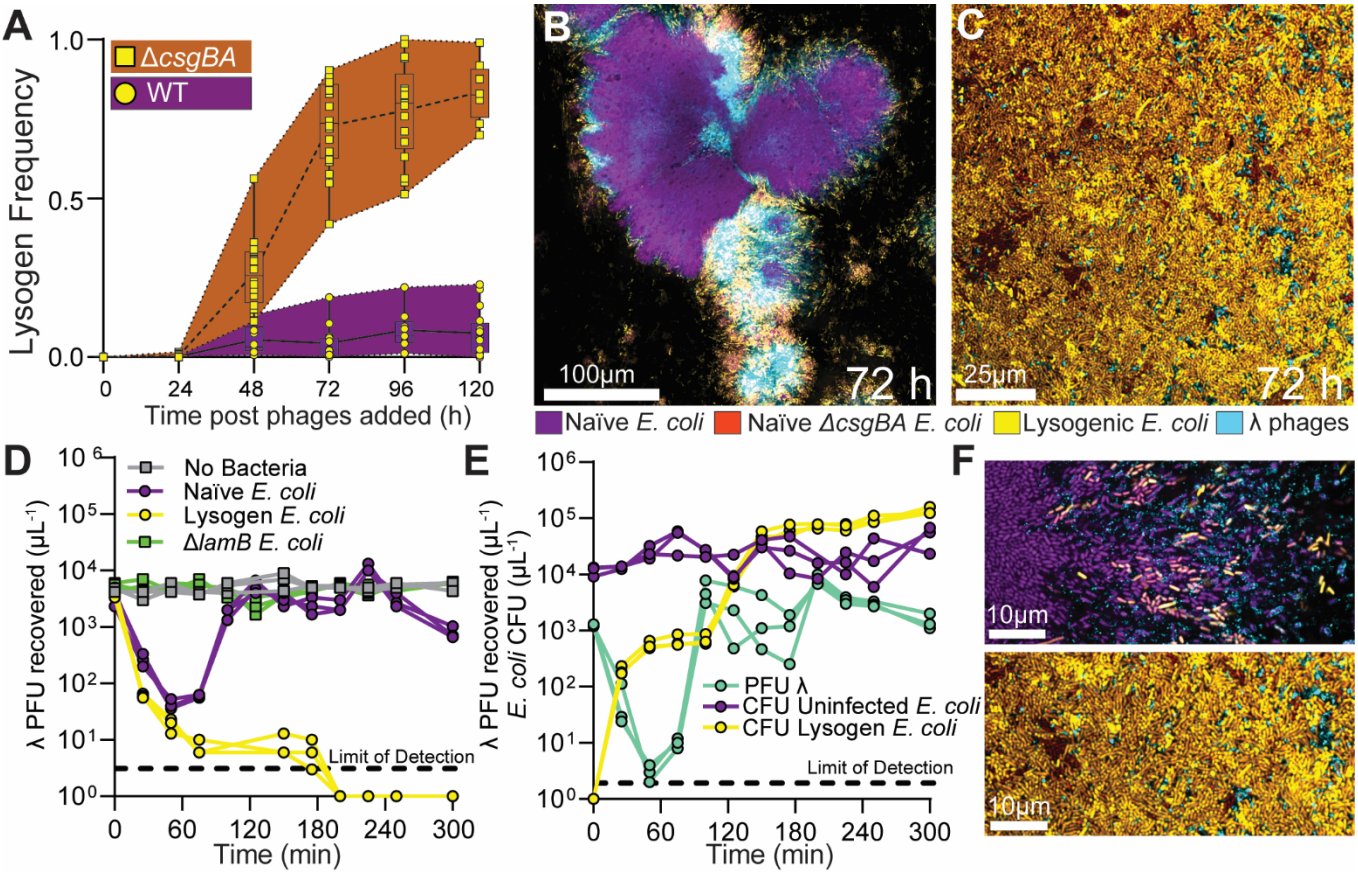

Figure 2. (A) Frequency of lysogens among all bacterial cells for WT and Δ*csgBA* (n = 9–20, n =7-20, respectively) biofilms during 120 h of continuous phage introduction. Error bars indicate the full data range. (B, C) Representative images of biofilms of WT and Δ*csgBA*, respectively, after 72 h of phage introduction. (D) PFU recovered after incubation of starting λ phage inoculum with either no bacteria, *E. coli* WT, Lysogenic *E. coli*, or *E. coli* Δ*lamB* over a 300-min time course. *E. coli* Δ*lamB* does not allow for λ phage attachment. Each trajectory shows the data for 1 run of each treatment (n = 3 for each treatment, giving 3 traces per treatment, with 3 technical replicates averaged for each time point). (E) PFU and CFU recovered after incubation of λ phage with WT *E. coli* over a 300-min time course. Each trajectory shows the data for 1 run of each treatment (n = 3 for each treatment, with 5 technical replicates averaged for each time point for CFUs, and 3 technical replicates averaged for each time point for PFUs). Lysogenic colonies were also differentiated from naïve colonies by selective plating. (F) Representative images of biofilms with cellular scale resolution of WT and Δ*csgBA*, respectively, after 72 h of phage introduction.

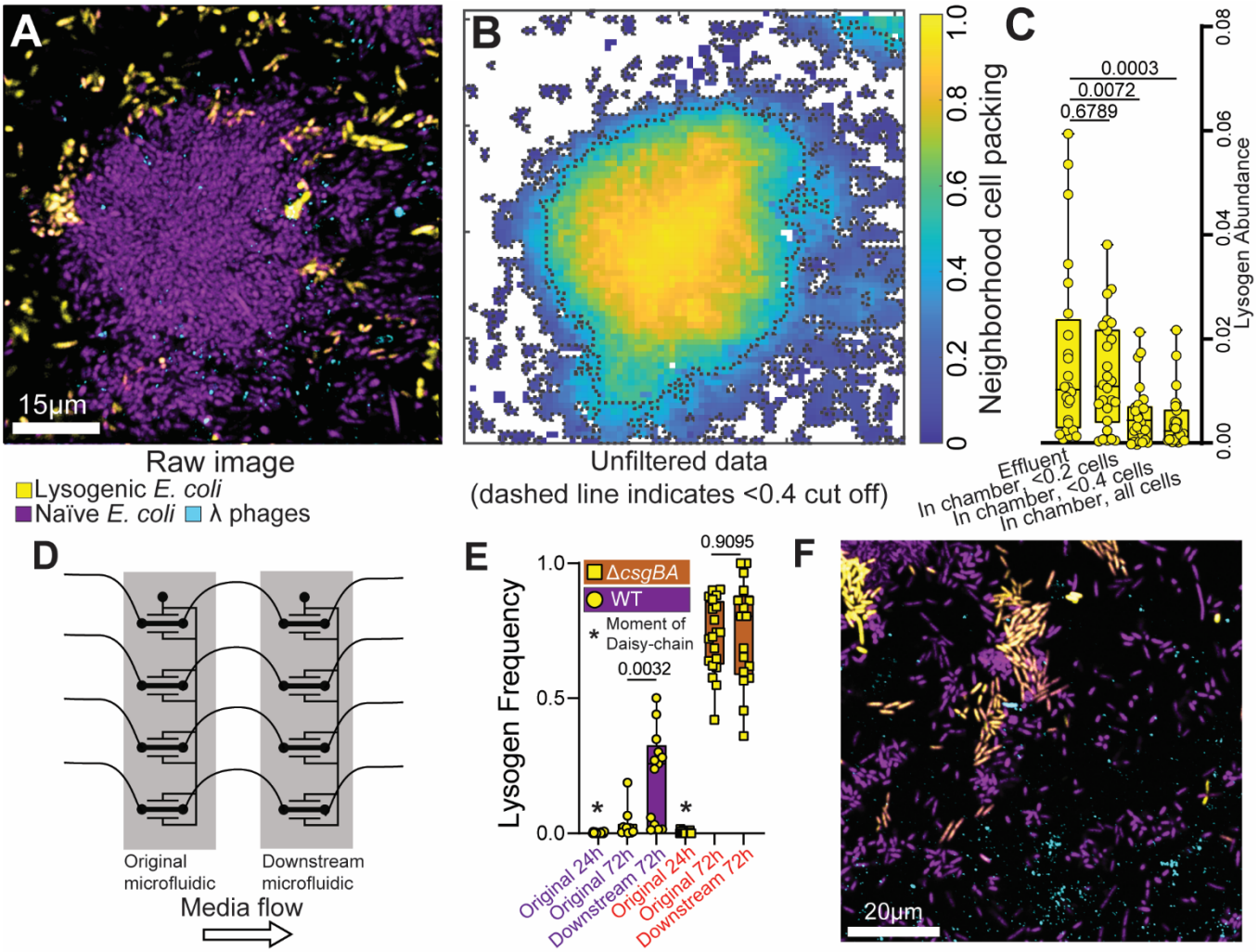

Figure 3. (A) Representative image of an *E. coli* biofilm that has been invaded with λ phages for 24 h. (B) Heatmap of the raw image of (A), plotting neighborhood cell packing within a 6µm radius. The dashed line indicates the <0.4 neighborhood cell density cut off, where any cell residing in regions of cell packing higher than 0.4 will be removed from quantification. (C). Lysogen frequency in the effluent and in the microfluidic devices at different cell-densities (n = 24–26). (D) Cartoon schematic of dispersal of biofilms into downstream microfluidic chambers. (E) Lysogen frequency in the original and downstream chambers for both WT biofilms and Δ*csgBA* biofilms at different timepoints (n = 10–20). (F) Representative image of a downstream WT *E. coli* biofilm. Statistical tests shown are Mann-Whitney U tests with a Bonferroni correction to account for unpaired, non-normally distributed, data collected.

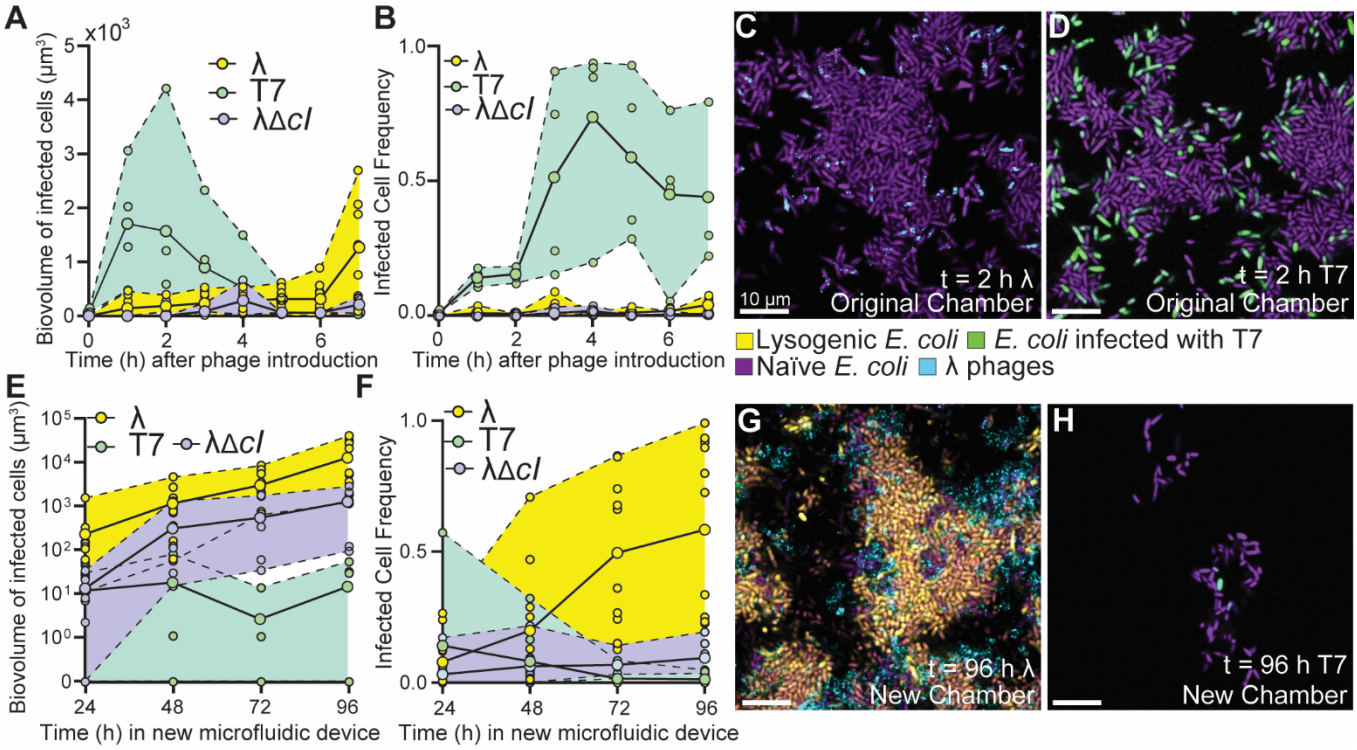

Figure 4. (A) Biovolume of infected cells in original (upstream) microfluidic devices for 7 h of phage exposure to either T7, λ, or λΔ*cI* phages (n=4-8). (B) Biovolume of infected cells in new (downstream) microfluidic devices over a 96 h time course (n=4-8). (C, D) Representative images of t = 2 h of exposure to λ or T7
765 phages, respectively. (E) Infected cell frequency as a proportion of the whole population for T7 or λ in original (upstream) microfluidic device (n=4). (F) Infected cell frequency in new (downstream) microfluidic devices (n=4-8). (G, H) Representative images of t = 96 h in the new microfluidic devices.

Supplemental Information

Spatial propagation of temperate phages within and among biofilms

James B. Winans[1], Sofia L. Garcia[1], Lanying Zeng[2], Carey D. Nadell[1*]

1. Department of Biological Sciences, Dartmouth, Hanover, NH

2. Department of Biochemistry and Biophysics, Center for Phage Technology, Texas A&M University, College Station, TX

* Author for correspondence:

Carey Nadell (ORCID 0000-0003-1751-4895)

carey.d.nadell@dartmouth.edu

78 College St., Rm. 326

Dartmouth, Dept. of Biological Sciences

Hanover, NH 03755

Author contributions

JBW and CDN conceptualized the study. CDN supervised the study. JBW led protocol design and experimental development. LZ contributed key reagents. JBW and SLG performed the experiments. JBW conducted data analyses and made the figures. JBW and CDN wrote the manuscript. JBW, SLG, LZ, and CDN edited the manuscript.

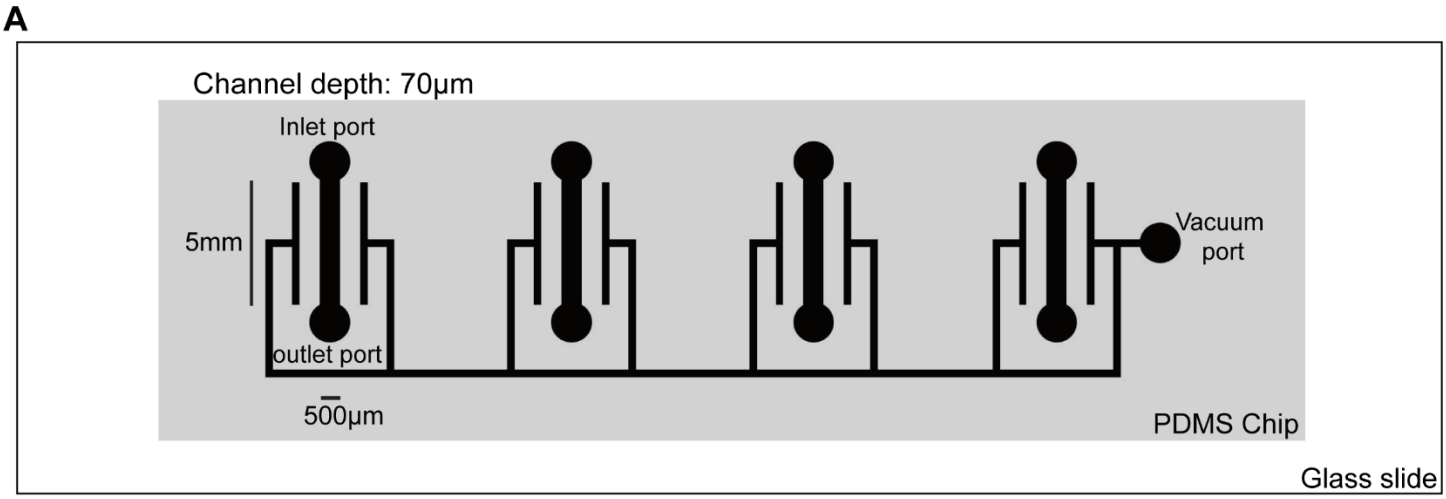

SI Figure 1 – (A) This example contains 4 parallel chambers, each with an inlet and an outlet port for connection to fluid inlet/outlet tubing. Technical replicate image stacks were taken from within the straight rectangular section between the rounded inlet and outlet ports of a chamber. The thinner, continuous channel surrounding the 4 separated chambers was connected to a wall vacuum line to apply negative pressure; this method discourages the introduction of air bubbles into the liquid-filled portions of the flow chambers.

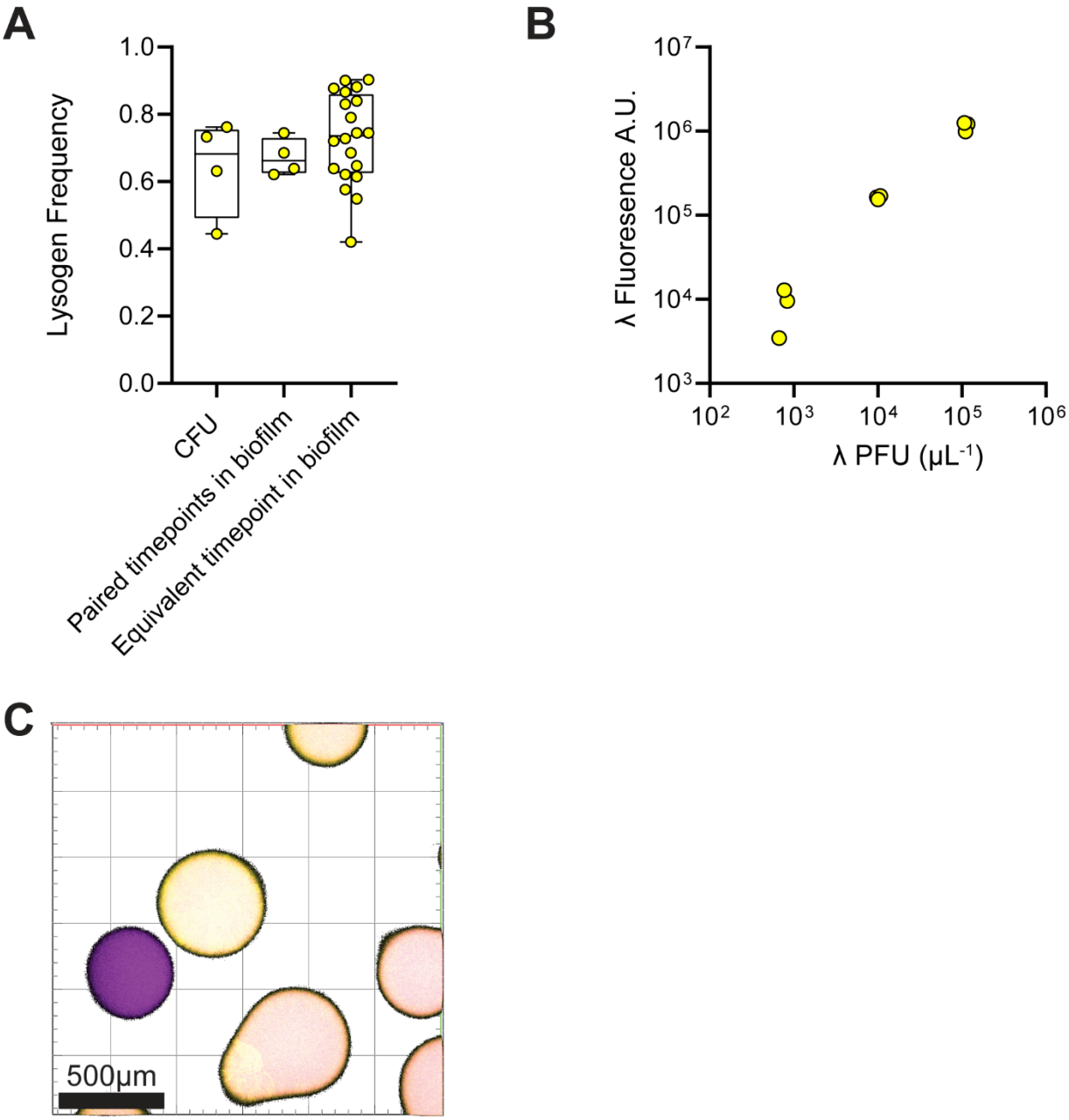

SI Figure 2 – (A) Lysogen frequency measured by CFU selective plating after mass dispersal of biofilms from the microfluidic devices, compared to the lysogen frequency observed in the microfluidic devices measured by image quantification with BiofilmQ (n = 4–20). (B) λ phage fluorescence quantified with BiofilmQ correlates with λ PFU linearly (n=9) (C) Lysogenic *E. coli* colonies on LB agar plates can be distinguished from naïve *E. coli* colonies by fluorescence.

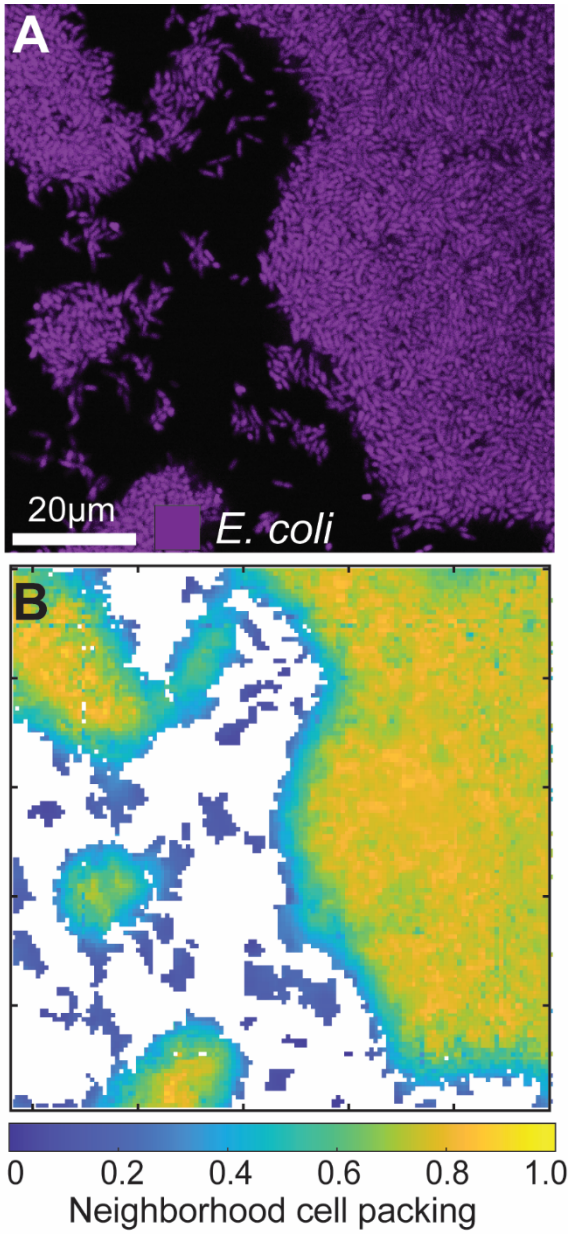

SI Figure 3 – (A) Representative image of an *E. coli* biofilm prior to the addition of λ phages. (B) Heatmap of neighborhood cell packing of (A), showing the variation often seen in *E. coli* biofilm formation dependent on growth stage.

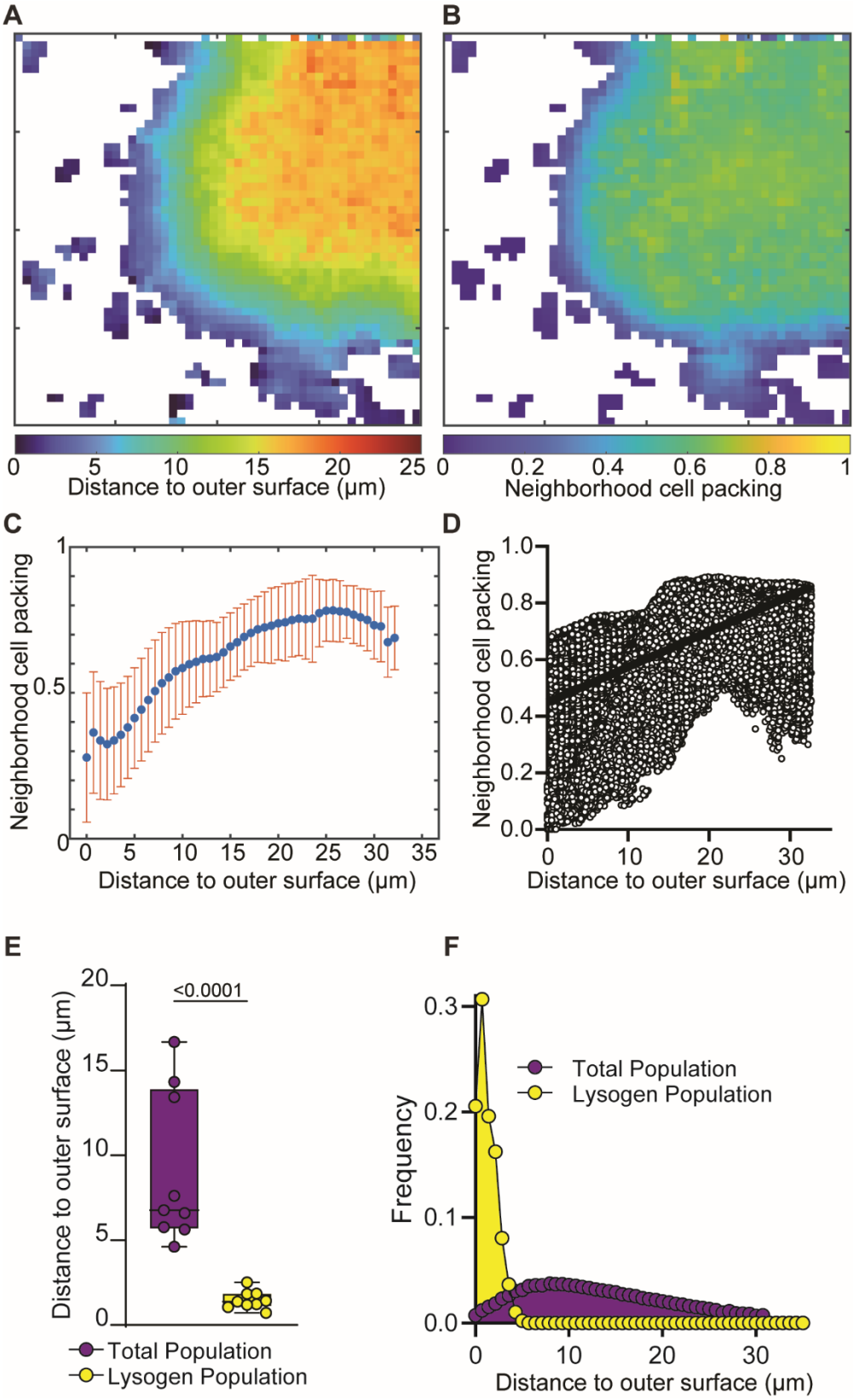

SI Figure 4 – (A) Representative heatmap of distance to outer surface (μm). (B) Representative heatmap of neighborhood cell packing for the same image data as (A). (C) 1.5D Histogram of neighborhood cell packing as a function of distance to outer surface (n=9). (D) Scatterplot of all of the cubes from image data sampled different microfluidic devices (n=9, total cubes=234,695) Black line represents simple linear regression fit to the data. (E) Average distance to outer surface for the total population and the lysogen population (n=9). (F) Frequency distribution of distance to outer surface for both populations (n=9).

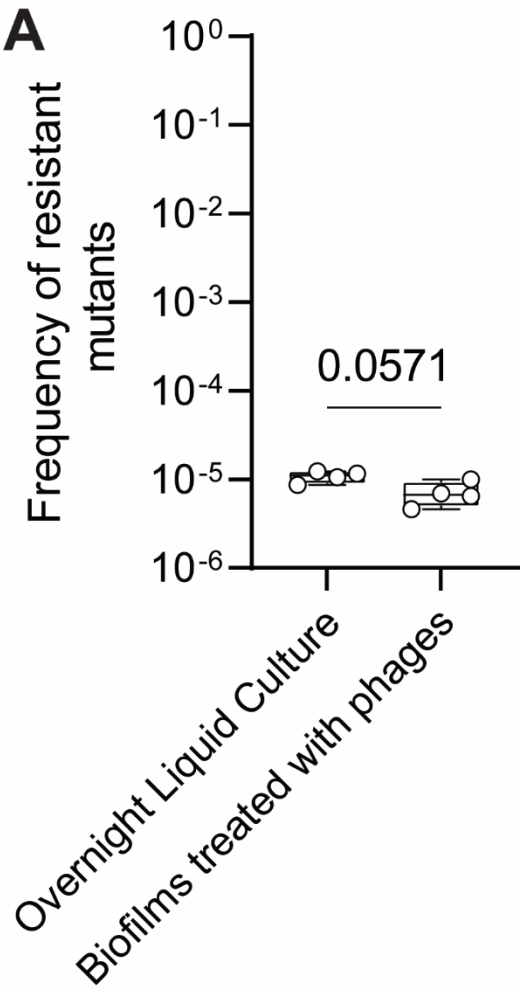

SI Figure 5 – *E. coli* was grown for 16 h in LB media at 37Cº overnight. We then plated for CFUs in the absence of phage, and simultaneously incubated *E. coli* with λΔ*cI* phages for 30minutes prior to plating onto soft agar. We then grew *E. coli* biofilms for 48 h, treated them with λΔ*cI* phages for 24 h, then flushed the chambers as described in (Methods). We then incubated *E. coli* with λΔ*cI* phages and plated onto soft agar for resistant colony formation. We found no difference in the frequency of resistant mutants.

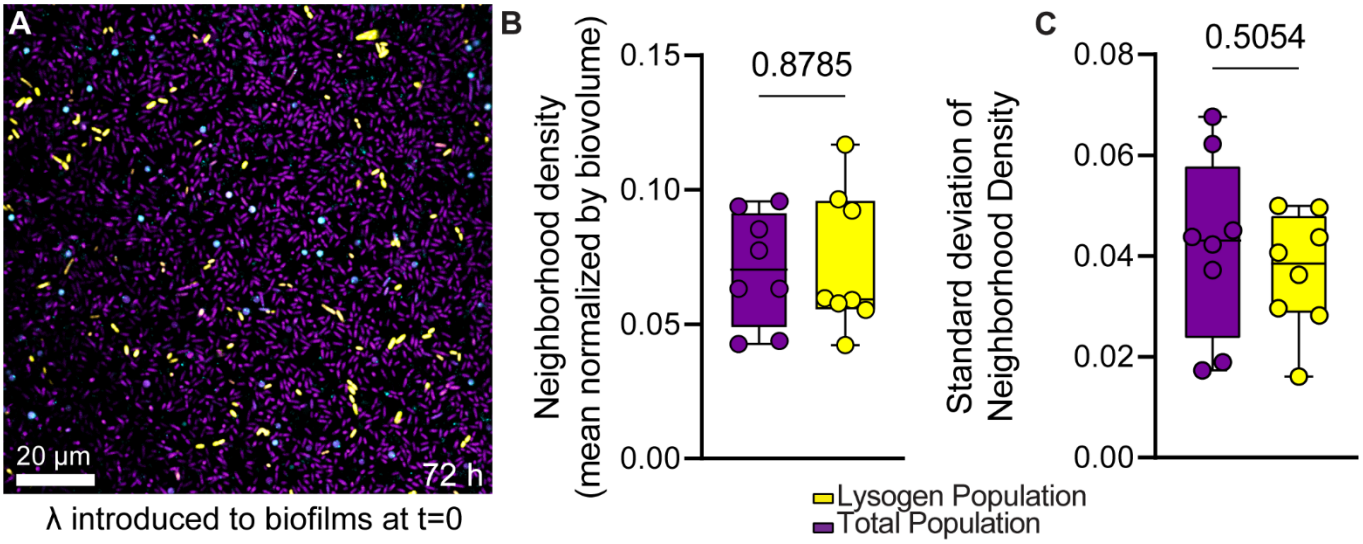

SI Figure 6 – (A) λ phages introduced to *E. coli* biofilms at t=0 (i.e. at the same time as bacterial inoculation) do not exhibit the characteristic pattern of phage spread and lysogenization as observed in established WT *E. coli* biofilms. (B) Neighborhood density of the total population compared to the lysogenic population, which are not significantly different (n=8). (C) The standard deviation of total population versus lysogenic population, also not significantly different (n=8).

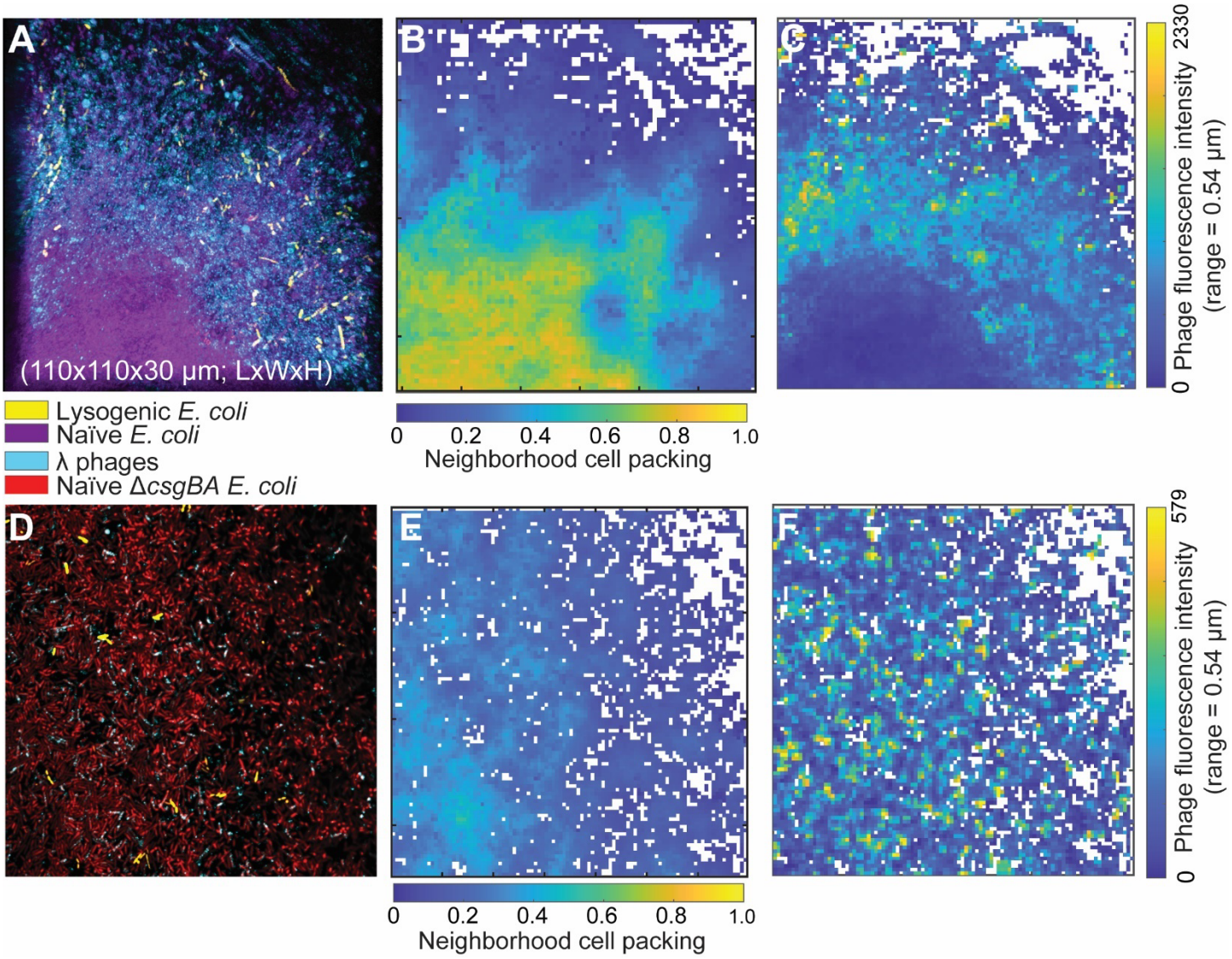

SI Figure 7 – (A) WT *E. coli* biofilm invaded with λ phages for 24 h. (B) Heatmap of neighborhood cell packing of the established biofilm. By visual inspection, the lysogens aggregate in a region of medium-low cell packing. (C) Heatmap of phage fluorescence intensity surrounding *E. coli.* (D) Δ*csgBA E. coli* biofilm invaded with λ phages for 24 h. (E) Heatmap of neighborhood cell packing of the established biofilm, with little spatial patterning of lysogenic cell aggregation. (F) Heatmap of phage fluorescence intensity surrounding *E. coli.*

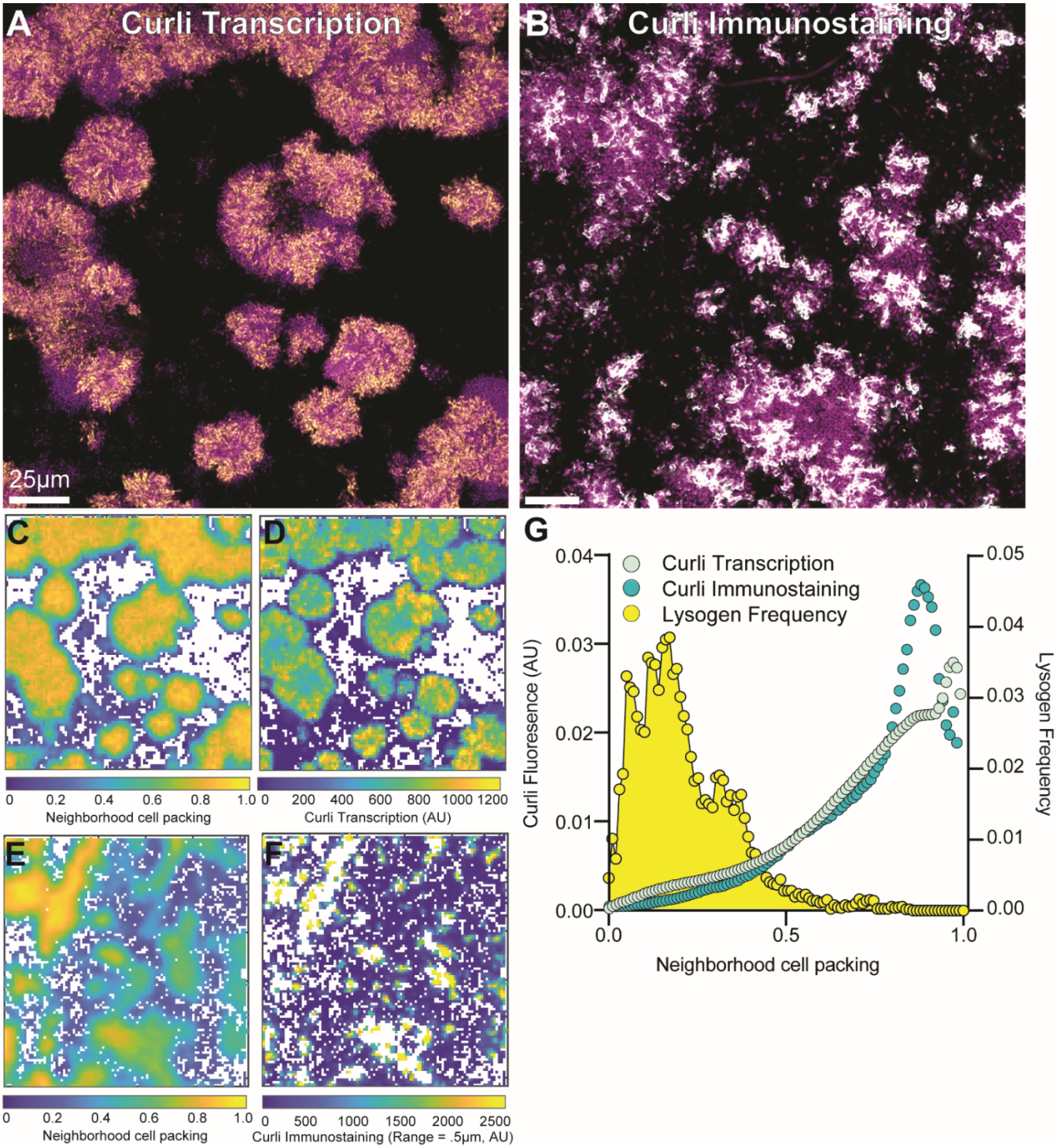

SI Figure 8 – (A) Representative image of *E. coli* (purple) containing the transcriptional reporter for the *csgBAC* operon (fluorescence from the reporter is shown in yellow). (B) Representative image of *E.coli* (purple) with fluorescent immunostaining of CsgA-6xHis produced from the native genomic locus (immunofluorescence shown in white). (C) Neighborhood cell packing of biofilms shown in panel (A). (D) Curli transcription heatmap of panel (A). (E) Neighborhood cell packing of biofilms shown in panel (B). (F) Shell fluorescence intensity with a range of .5μm around *E. coli* cells, staining for curli-associated immunofluorescence. (G) Curli transcription and immunostaining fluorescence intensity as a function of neighborhood cell packing from independent replicates (n=12, n=8, respectively). Lysogen frequency as a function of biofilm cell packing (yellow distribution) denotes the same data as used in Figure 1 of the main text.

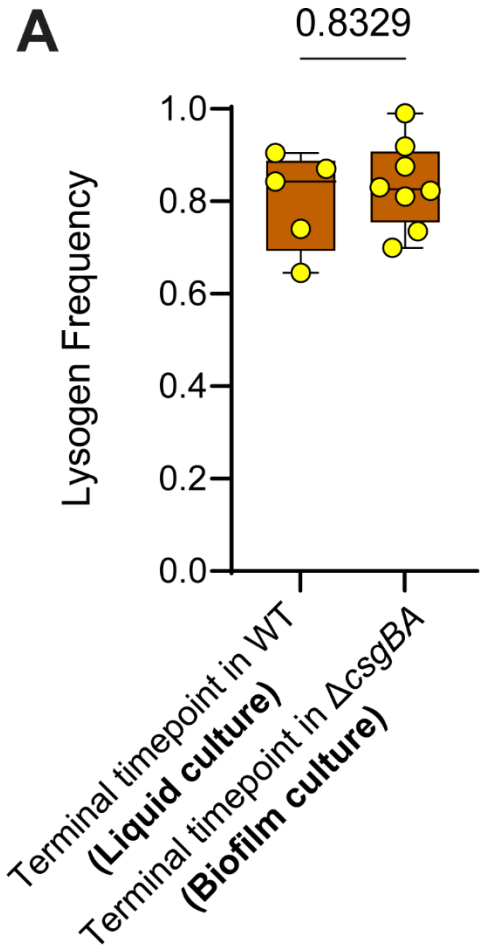

SI Figure 9 – (A) Lysogen frequency within our well-mixed liquid culture conditions were not significantly different from our lysogen frequency in microfluidic device culture of Δ*csgBA* biofilms (n = 5–9). P-values are shown for Mann-Whitney U-tests for pairwise comparison.

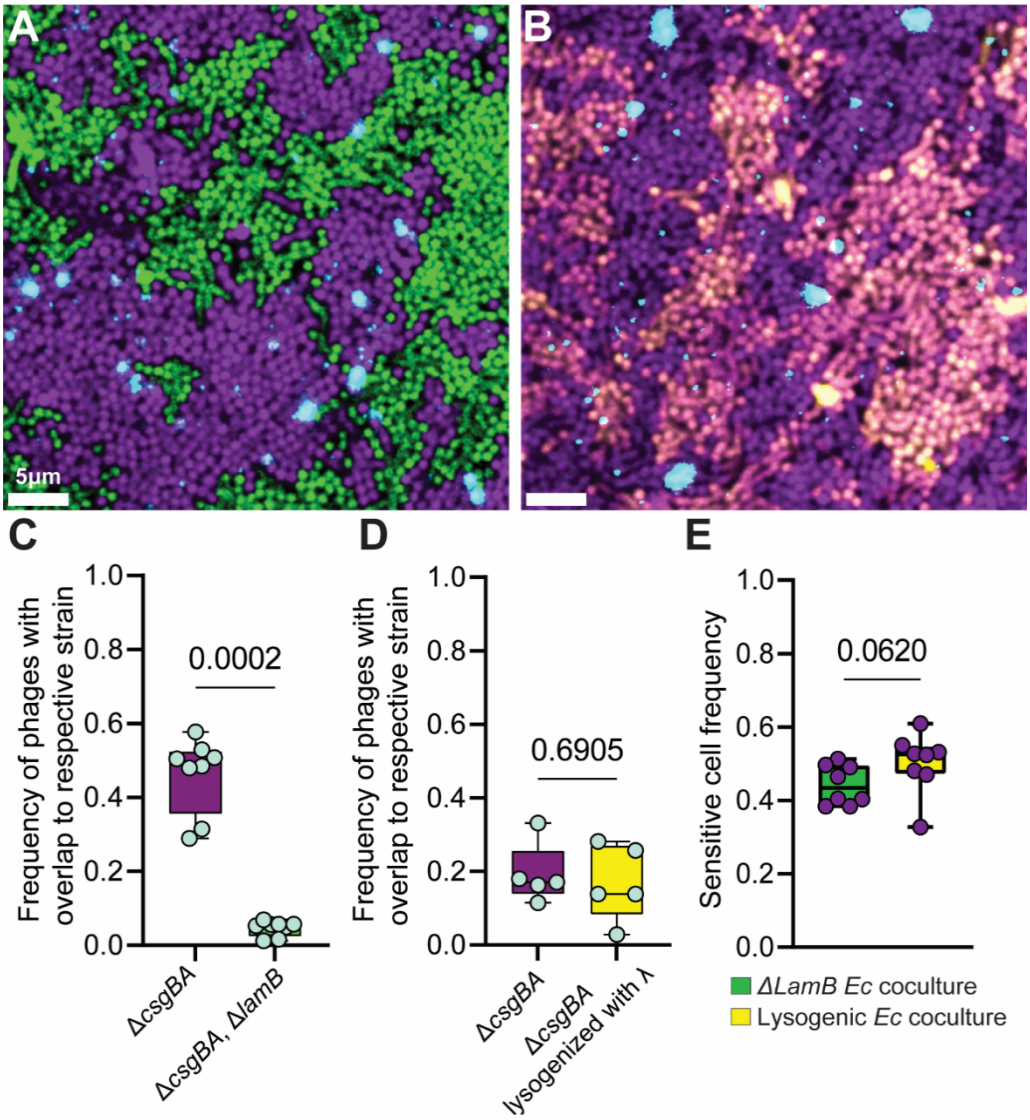

SI Figure 10 – (A) Coculture biofilms of of Δ*csgBA* (purple) and Δ*csgBA, ΔlamB* (green), inoculated with λ phages (Turquoise) for 24 h. (B) Coculture of Δ*csgBA* (purple) and Δ*csgBA* lysogens (yellow) with phage λ (cyan), inoculated with λ phages for 24 h. (C) Frequency of phages with positive Manders' overlap for Δ*csgBA* and Δ*csgBA* and Δ*lamB* (n=8) (D) Frequency of phages with positive Manders' overlap for Δ*csgBA* and Δ*csgBA* lysogenized with λ (n=5). (E) Sensitive cell frequency in the two separate coculture experimental setups (n=8). P-values are shown for Mann-Whitney U-tests for pairwise comparison.

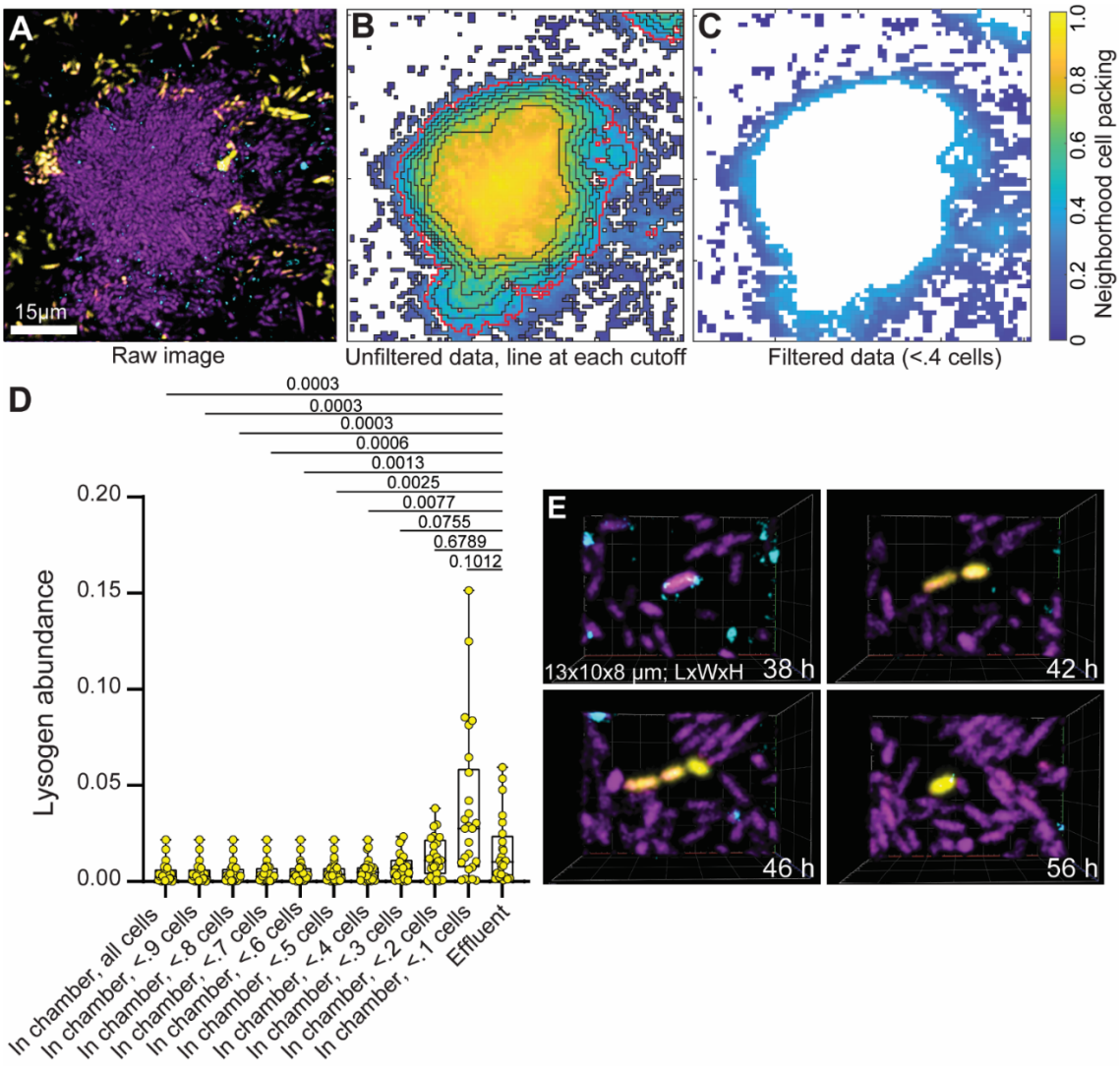

SI Figure 11 – (A) Representative image of a biofilm chamber location when effluent was collected. (B) heatmap of neighborhood cell packing density for the biofilm in panel (A), with lines denoting a range of density threshold cutoffs, with the 0.4 line highlighted in red. (C) Corresponding heatmap of neighborhood density of in panel (A), but with any cell volumes with cell packing >0.4 been removed. (D) Lysogen abundance on a continuum of local densities compared to the effluent of the microfluidic device. Pairwise comparisons are Mann-Whitney U test with Bonferroni correction. For 10 comparisons, an adjusted critical α value is 0.005. (E) Timelapse of a sensitive *E. coli* cell (purple) infected with λ (Turquoise) at 38 h and becoming lysogenized (yellow). We observed two division events before dispersal from the microfluidic device.

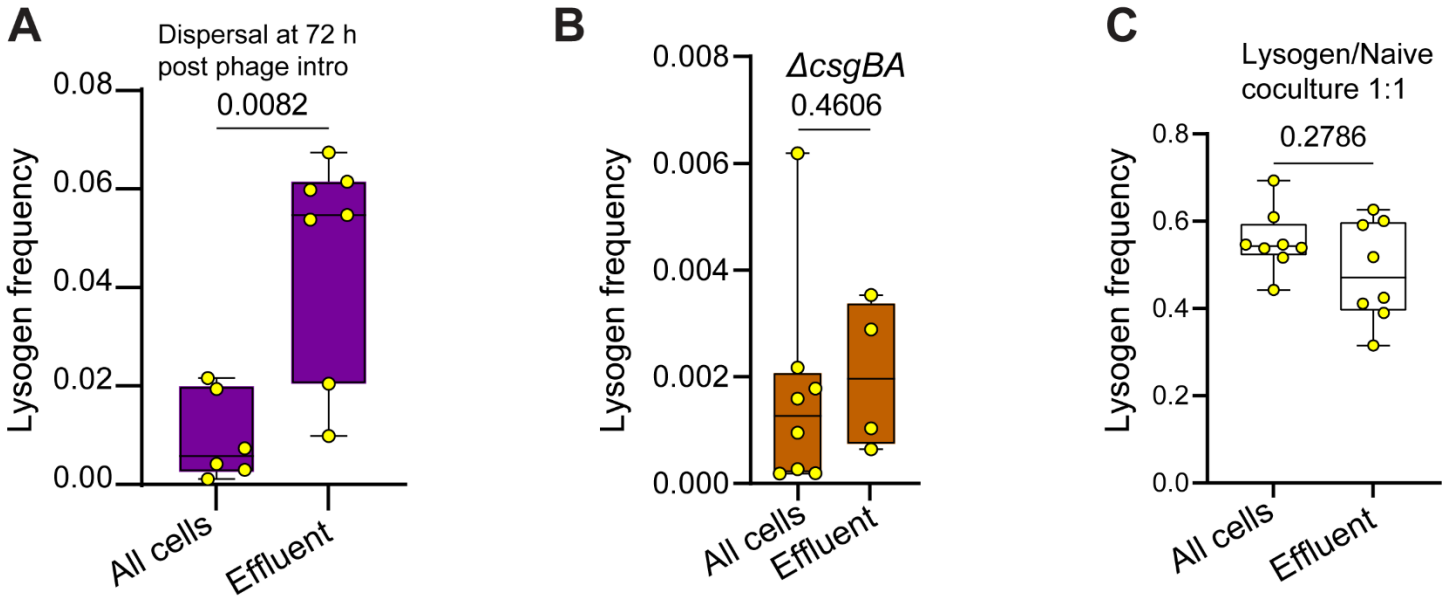

SI Figure 12 – (A) Lysogen frequency of WT *E. coli* biofilms that have been invaded with λ phages for 72 h (n=6-7). (B) Lysogen frequency in Δ*csgBA* microfluidic device biofilms and dispersing effluent (n=4-8). (C) Lysogen frequency in the total biofilm population and in the dispersing effluent population from 72 h biofilms in which lysogens and naïve WT *E. coli* cells were inoculated at a 1:1 ratio from the beginning of biofilm growth (n=8). Statistical tests shown are Mann-Whitney U tests.

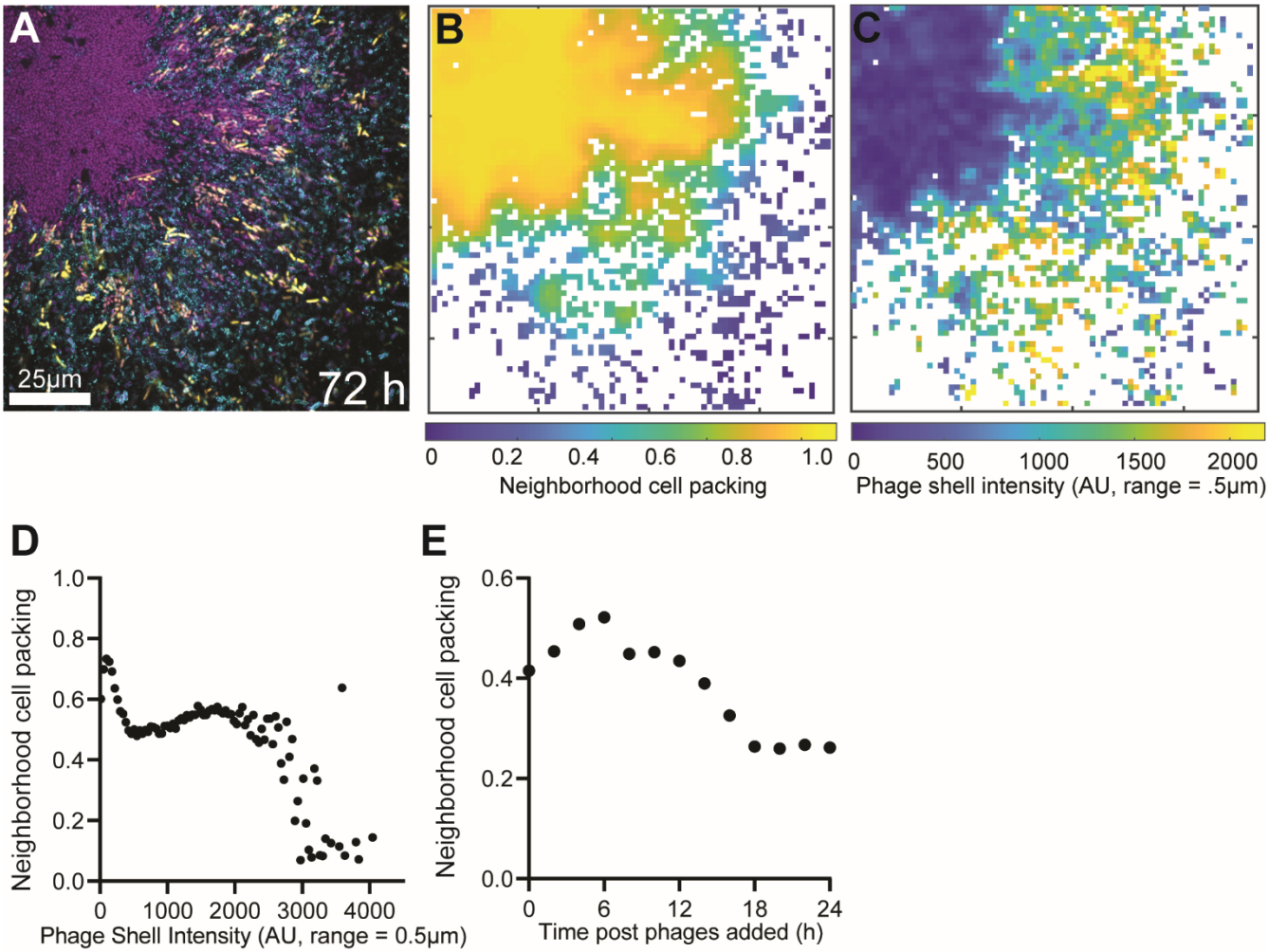

SI Figure 13 – (A) Representative image of an *E. coli* biofilm exposed to phages for 72 h. Naïve *E. coli* hosts are shown in purple, phages in cyan, and lysogens in yellow. (B) Corresponding heatmap of neighborhood cell packing for the biofilms shown in panel (A). (C) Corresponding phage shell fluorescence intensity around each segmented *E. coli* volume within a 0.5μm radius. (D) Neighborhood cell packing as a function of phage shell intensity, showing a negative relationship. (E) Data from a high resolution timelapse showing changes in neighborhood cell packing 24 h after phages have been introduced to the biofilm. Cell packing decreases over time due to phage activity on the periphery of biofilm clusters.

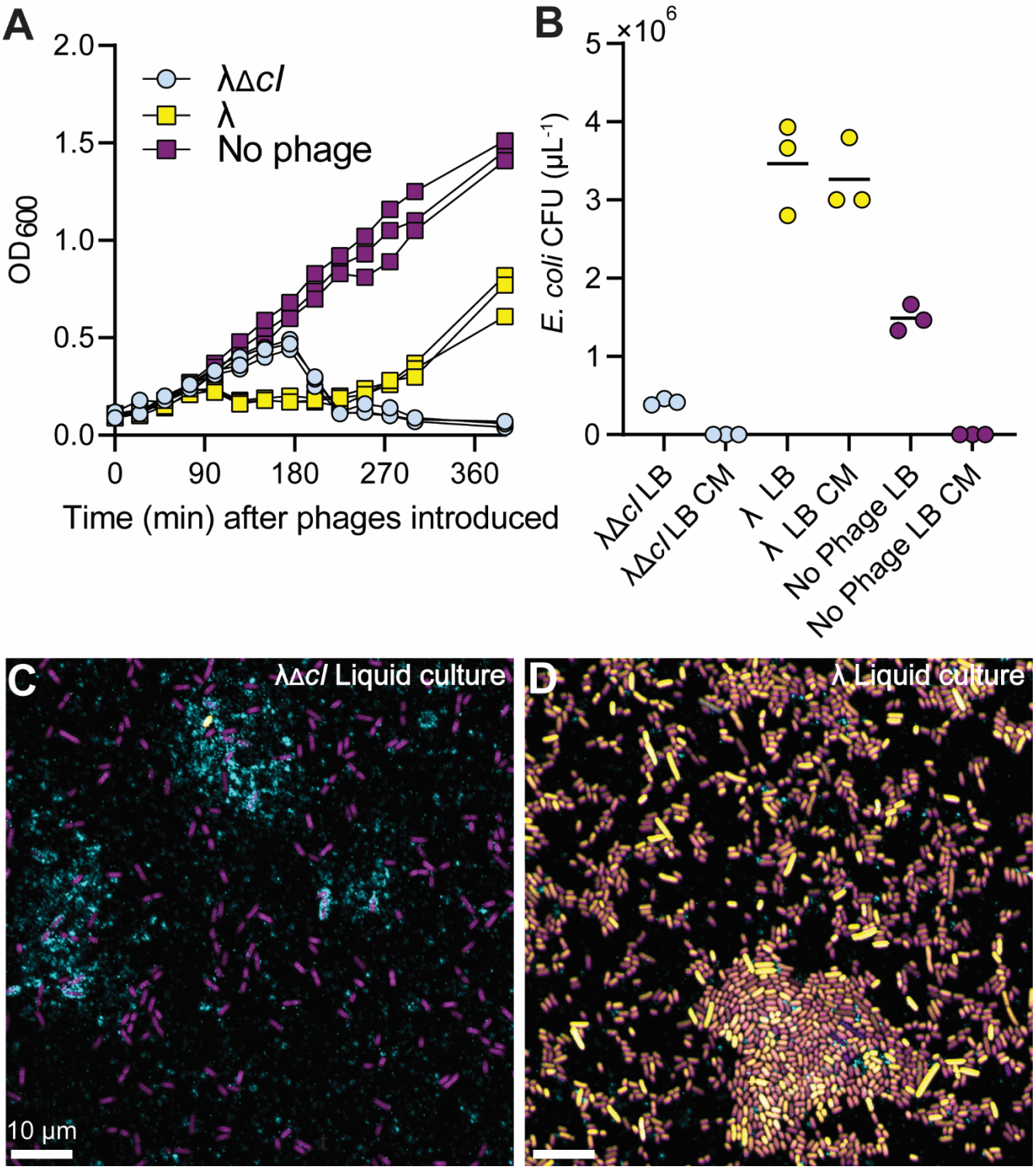

SI Figure 14 – (A) OD_{600} curve of exponentially growing *E. coli* in λ broth, inoculated with λ or λΔ*cI* and grown at 30Cº. After a lag period relative to the no-phage control, we observe an increase in OD_{600} of lysogens after addition of phage λ, but no increase in population density after addition of the obligately lytic phage derivative λΔ*cI*. (B) Colony Forming Units (CFUs) of *E. coli* on LB plates or LB + chloramphenicol (CM) plates after incubation with λ, λΔ*cI*, or no phage in LB media for 24 h, a separate experimental setup from that shown in panel (A). Our strain of phage λ contains a chloramphenicol resistance marker, so lysogens are Cm resistant. (C,D) Images of a sample taken from the λΔ*cI*/*E. coli* liquid culture and λ/*E. coli* liquid culture after 24 h.